

ALPHA PARTICLE LOSS IN THE TFTR DT EXPERIMENTS

S.J. ZWEBEN¹, D.S. DARROW¹, H.W. HERRMANN¹, S.H. BATHA²,
R.V. BUDNY¹, C.-S. CHANG³, Z. CHANG¹, E.D. FREDRICKSON¹,
D.L. JASSBY¹, L.C. JOHNSON¹, F.M. LEVINTON², H.E. MYNICK¹,
D.K. OWENS¹, J.F. SCHIVELL¹, S.D. SCOTT¹, M.H. REDI¹,
J.D. STRACHAN¹, K. TOBITA⁴, K.M. YOUNG¹

¹ Princeton Plasma Physics Laboratory, Princeton University, Princeton, New Jersey, United States of America

² Fusion Physics and Technology, Torrance, California, United States of America

³ Courant Institute, New York University, New York, United States of America

⁴ JAERI, Fusion Research Establishment, Naka-machi, Naka-gun, Ibaraki-ken, Japan

ABSTRACT. Alpha particle loss was measured during the TFTR DT experiments with a scintillator detector located at the vessel bottom in the ion ∇B drift direction. The DT alpha particle loss to this detector was consistent with the calculated first orbit loss over the whole range of plasma current $I = 0.6$ – 2.7 MA. In particular, the alpha particle loss rate per DT neutron at a given plasma current did not increase significantly with fusion power up to 10.7 MW, indicating the absence of any new ‘collective’ alpha particle loss processes in these experiments.

1. INTRODUCTION

One alpha particle is created for each neutron in the fusion reaction



A tokamak reactor will use the alpha particle power for heating, and will ignite only when the alpha power being transferred to the plasma exceeds the plasma energy loss rate. To ensure ignition in a tokamak, the alpha particles must be well confined during their thermalization, for example, for a time-scale on the order of 1 s in ITER.

In an ideal, axisymmetric, MHD-quiescent tokamak the alpha particle confinement should be dominated by the finite orbit width of the alphas, which leads to ‘first-orbit’ loss of the fat banana orbits. Globally, this loss is typically <5% when the plasma current is above $I = 2$ MA (see Appendix A), which represents a negligible loss of alpha heating. However, a stricter constraint on alpha particle loss will be set by the need to protect the mechanical structures on the first wall of a reactor from potentially localized alpha heating [1]. Thus, some understanding of the location of this alpha loss is needed to design the appropriate first wall armour and cooling, even if the alpha loss is only a few per cent globally.

Previous tokamak experiments have simulated DT alpha particle confinement and loss using other fusion

products such as the 1 MeV tritons from DD, or the fast ions used for auxiliary heating [2]. The usual conclusion from these experiments is that fast ions are generally well confined and thermalize ‘classically’ in the absence of large MHD activity, i.e. the ion loss is determined solely by the static magnetic fields of the plasma current and toroidal field (TF) ripple. However, large MHD activity in TFTR and other tokamaks has been shown to cause a fast ion loss fraction of up to $\approx 50\%$, which would be intolerably large for a reactor. As discussed in the comprehensive review in Ref. [2], such MHD induced fast ion loss can either be a ‘single particle’ effect driven by the background plasma fluctuations (e.g., due to low m/n kink tearing modes), or a ‘collective’ effect driven by the fast ion population itself (e.g., neutral beam driven TAE modes). One of the main motivations for the TFTR DT experiments was to explore any new collective alpha particle driven MHD activity in DT, and to measure its effect on the alpha particle loss [3, 4].

This paper presents a detailed description of the TFTR alpha particle loss measurements made between the first DT experiments in December 1993 and the achievement of 10.7 MW of DT fusion power in November 1994. The measurements described here were made with a lost alpha detector located 90° below the outboard midplane in the ion ∇B drift direction. The main result of this paper is that there was *no* observable new collective alpha particle loss during

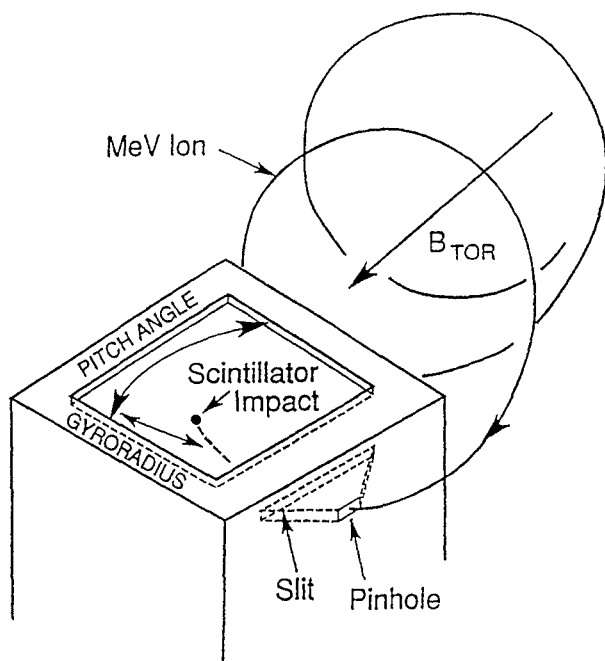


FIG. 1. Schematic diagram of the design of the TFTR lost alpha detector, which was located 90° below the outboard midplane. The escaping alphas enter a pair of apertures that disperse them in pitch angle and gyroradius. The 2-D image of the visible light emission from the scintillation screen is transmitted through a quartz fibreoptic bundle to a gated intensified video camera for analysis.

these initial DT experiments. This is consistent with the observations that no new Alfvén frequency fluctuation activity [5] or increased plasma losses [6] were observed in these DT plasmas. More detailed discussions of the results from the other alpha loss detectors (60° , 45° and 20° below the outer midplane), and of the occasional time-dependent MHD-induced alpha loss fluctuations, will be presented elsewhere.

2. PREVIOUS EXPERIMENTS ON FUSION PRODUCT LOSS IN TFTR

A schematic diagram of the lost alpha detector is shown in Fig. 1. The alpha detector element was a scintillator screen enclosed in a light tight box located near the vessel wall, but well outside the plasma. The detector used here was located 90° poloidally below the outer midplane at a toroidal location between two TF coils. It was fixed in the vessel with its aperture on a field line less than 1 cm radially outward from the nearest poloidal limiter, after taking into account the small field line movement due to TF ripple. This was close enough to avoid any shadowing of the escaping

first orbit alpha loss by this limiter, which was about 2 m away toroidally.

The pinhole/slit aperture pair shown in Fig. 1 allowed fast ions with gyroradii in the range ≈ 2 –12 cm to hit the scintillator screen, resulting in a visible light image that was optically transferred to an intensified CCD camera using a quartz lens and coherent fibre-optic bundle underneath the vessel. The ‘pinhole’ entrance aperture dimensions are about 1 mm high by 2 mm wide, while the slit was 1 mm high by 1.5 cm wide, 1 cm behind the pinhole. A $3\ \mu\text{m}$ aluminium foil behind the slit set the lower limit of detectable alpha energy to be ≈ 1 MeV. The hardware and calibration of this system have been described elsewhere [7–10].

The two dimensional (2-D) scintillator light emission patterns were analysed and interpreted using a detector simulation code that calculated the expected scintillator images of fast ions incident at a given pitch angle and gyroradius, including the geometrical and optical resolutions of the system [11]. The pitch angle is defined here with respect to the local toroidal field B , with 90° being perpendicular to B , and 0° being along the co-I (plasma current) direction, and so is a measure of the ion’s magnetic moment at a given gyroradius. The alpha gyroradius as defined here is $\rho = (2E/M)^{1/2}/\Omega$, where E is the energy of an alpha with mass M and gyrofrequency Ω , i.e. the gyroradius is a measure of the ion’s energy. Typically 3.5 MeV alpha particles have a gyroradius of $\rho \approx 5.4$ cm at the 90° detector for the nominal $B = 5$ T toroidal field of TFTR (of course, this gyroradius varies with the local B at the detector).

This system has been used for several years to measure the loss of DD fusion products (3 MeV protons and 1 MeV tritons), which have gyroradii only $\approx 10\%$ less than those of the 3.5 MeV alphas from DT. Previous results can be summarized as follows:

- For MHD-quietest $R = 2.6$ m plasmas the loss to the 90° detector was consistent with the expected first orbit loss over the plasma current range $I = 0.6$ –2.0 MA [11].
- An additional anomalous delayed loss was seen at 90° for $R = 2.45$ m plasmas at $I = 1.4$ –2.5 MA [12].
- During large coherent MHD activity there was up to a factor of 3 increase in the losses at the 90° and 20° detectors [13].
- The pitch angle distributions of the loss at 60° and 45° agreed reasonably well with the first orbit model at $I = 1.2$ MA [14].
- There was a large non-first-orbit loss component in the 20° detector, which was consistent with the

expected loss due to stochastic TF ripple diffusion [15].

The non-classical features of these 'single particle' DD loss measurements were summarized recently to help isolate any new 'collective' alpha effects in the DT experiments [16].

Between the DD run in 1992 and the DT run in 1993 there were several changes to this lost alpha diagnostic. On the basis of measurements at the Los Alamos Van de Graaff accelerator [9], the scintillator material was changed from zinc sulphide (P11 or P31) to yttrium aluminate (P46), which is about 20 times less efficient, to guarantee the linearity and damage resistance of the phosphor at the ≈ 100 times larger ion flux levels expected in DT (estimated to be $\approx 10^{10}$ alphas/cm² on the scintillator for ≈ 1000 DT shots). In addition, the intensified video camera that recorded the light from the scintillators was moved to a shielded enclosure in the basement to avoid direct neutron noise (none was observed in DT), and additional shielding was added around the coherent quartz fibreoptic bundle under the vessel to minimize neutron induced background light generated in the quartz fibreoptic bundle (some was still seen) [10].

3. MODELLING OF ALPHA PARTICLE LOSS TO THE 90° DETECTOR

Calculations of the *local* first orbit loss to the 90° detector were made using an axisymmetric Lorentz code that calculated the exact trajectory of the alpha

particle from the detector backwards into the plasma, including its finite gyroradius and gyrophase [17]. Using this code, it was found that the first orbit alpha loss 90° below the outboard midplane depends mainly on the plasma current, which determines the displacement of the alphas from the flux surfaces of their birth.

Calculations of the *global* first orbit and TF ripple loss of alphas were not used for interpreting the localized experimental results in this paper, and so are summarized separately in Appendix A. However, one important result of these calculations is that TF ripple induced alpha loss is not expected at the 90° detector location, since the confined trapped alpha orbits which are affected by TF ripple are lost mainly near the outer midplane. Therefore first orbit loss is the dominant classical alpha loss process at the 90° detector location.

Typical first orbit alpha loss trajectories to the 90° as calculated by the Lorentz code are shown in Fig. 2. The $q(r)$ profiles for these analyses were taken from the TRANSP (time dependent) transport code, and were spot checked with the measured $q(r)$ profiles from the Motional Stark Effect (MSE) diagnostic, as described in Appendix B. The orbits shown in Fig. 2 are calculated 'backwards in time' from the detector to the plasma midplane for three different pitch angles at two different plasma currents (the actual trajectories are symmetrical above and below the midplane).

At the lowest current of $I = 0.6$ MA the 90° detector can 'see' alpha loss orbits from the whole alpha source profile, including the highest source rate region near the plasma centre. Therefore the total alpha loss at

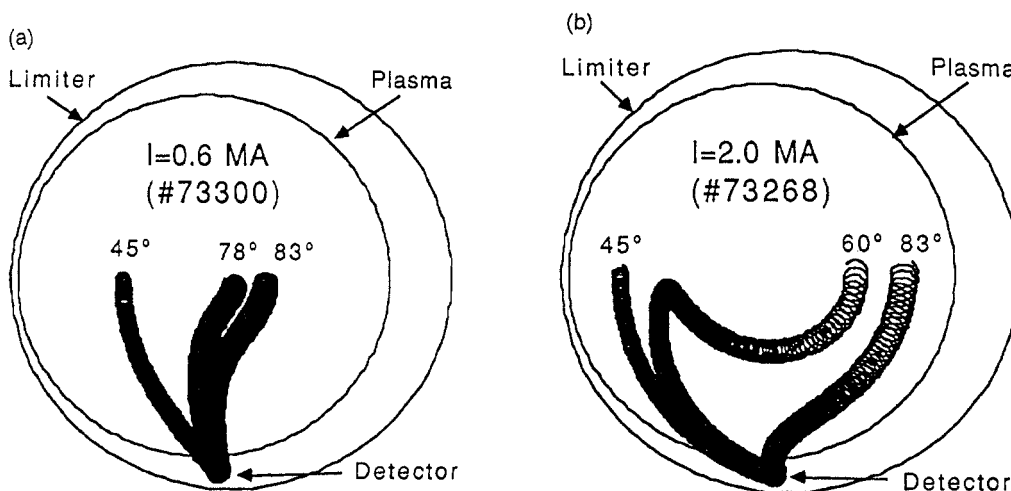


FIG. 2. Calculated loss orbits for 3.5 MeV alpha particles to the 90° detector in TFTR for plasma currents of (a) $I = 0.6$ MA and (b) $I = 2.0$ MA. At $I = 0.6$ MA this detector 'sees' first orbit alpha loss from the plasma centre, while at $I = 2.0$ MA it does not, which results in a lower alpha collection fraction at the higher current. The pitch angle of the maximum alpha loss is $\chi \approx 78^\circ$ at $I = 0.6$ MA, but $\chi \approx 60^\circ$ at $I = 2.0$ MA. These orbit plots are stopped at the midplane, but in reality are vertically symmetrical.

90° was found to be relatively insensitive to the $q(r)$ or alpha (i.e. neutron) source profiles at this current. Thus the alpha loss at $I = 0.6$ MA was used as an *in situ* calibration of the alpha loss at higher currents.

For the $I = 2.0$ MA case shown in Fig. 2(b) there is no first orbit loss to the 90° detector expected from the highest fusion source rate region near the plasma centre. The largest component of first orbit loss was from orbits near the ‘fattest’ banana at a pitch angle of $\chi = 60^\circ$, as shown. Therefore, the total first orbit alpha loss to the 90° detector at this current does depend on the assumed current profile, which determines the shape of the fattest banana orbit, and also on the alpha source profile, which determines the local alpha birth rate near the orbit’s closest approach to the plasma centre.

This Lorentz code calculates the expected first orbit alpha loss at a given pitch angle by calculating the alpha orbit, integrating the alpha source function along this loss orbit and correcting for the area, solid angle and orientation of the specific detector aperture pair [11]. The total ‘alpha collection fraction’ is defined here as the ratio between the alpha loss into the 90° detector (i.e. integrated over the aperture’s pitch angle and gyroradius acceptances) and the *global* alpha source rate. Thus the alpha collection fraction for this detector was typically $\approx 10^{-8} - 10^{-9}$, the scale of which is mainly set by the small size of the pinhole aperture (0.02 cm²) with respect to the area of the bottom of the TFTR vessel ($\approx 5 \times 10^5$ cm²).

4. ALPHA LOSS TO THE 90° DETECTOR

Most of the previous analyses of DD fusion product loss in TFTR were made with data from the detector 90° below the midplane [11–14]. This was mainly because this detector has the best optical coupling efficiency between the scintillator and the fibreoptic bundle, and so had the largest signal levels and the best resolution of the three fixed detectors. Also, since no TF ripple loss was expected at 90° (see Appendix A), the analysis of the expected loss to this detector was relatively straightforward. The DT results are described in Sections 4.1 to 4.8, and a summary of the corresponding DD results is in Section 4.9.

4.1. Plasma parameters

All of the discharges discussed in this paper occurred during the 1993–94 TFTR run period, which included both DT and the corresponding DD discharges for comparison. All these plasmas had the

same major and minor radii of $R = 2.52$ m, $a = 0.87$ m, respectively, and a toroidal field in the narrow range of $B = 4.8$ –5.1 T. Neutral beam injection was used with powers of 5–40 MW for 0.7–1.0 s in these ‘supershots’ (no ICRH was used here).

Table I summarizes the main parameters of this data set, sorted according to their plasma current. The 40 DT discharges came from four types of experiment:

- (a) Experiments at $I = 2.0$ MA with a small tritium fraction ($\approx 2\%$) in all the neutral beam injectors (NBI);
- (b) A plasma current scan over $I = 0.6$ –1.8 MA with a single tritium beam source, i.e. 2.5 MW of T beams;

TABLE I. SHOT LIST

(DT shots in boldface, ≈ 2.5 MW for each beam source)

Shot No.	Current (MA)	NBI power (MW)	Beams #T/#D	Neutron rate ($\times 10^{17}/s$)
73300	0.6	5	1/1	0.45
73301	0.6	5	1/1	0.48
73302	0.6	5	1/1	0.48
72988	0.6	5	0/2	0.01
72989	0.6	5	0/2	0.01
73311	1.0	10	1/3	1.90
73312	1.0	10	1/3	1.80
72993	1.0	10	0/4	0.05
73314	1.4	10	1/3	2.38
73315	1.4	10	1/3	2.40
72994	1.4	10	0/4	0.06
73306	1.8	13	1/4	3.13
73307	1.8	13	1/4	3.27
73446	1.8	22	5/3	13.10
73447	1.8	21	7/0	7.86
73450	1.8	23	8/0	9.55
73452	1.8	20	5/2	11.00
73457	1.8	20	2/6	7.83
72990	1.8	10	0/4	0.03
72991	1.8	15	0/6	0.08
73222	2.0	13	1/4	3.00
73228	2.0	8	1/2	2.20
73229	2.0	6	1/1	1.20
73234	2.0	28	1/10	6.80
73235	2.0	24	4/5	14.30
73254	2.0	27	4/6	14.90
73258	2.0	27	5/5	16.10
73268	2.0	29	7/4	20.30
73273	2.0	22	7.5/0	7.90
72635	2.0	19	8/0*	0.76
72695	2.0	20	5.5/3*	0.51
73219	2.0	13	0/5	0.10
73220	2.0	13	0/5	0.10

TABLE I. Cont.

Shot No.	Current (MA)	NBI power (MW)	Beams #T/#D	Neutron rate ($\times 10^{17}/s$)
76746	2.5	24	4/4	15.00
76747	2.5	27	5/4	20.00
76748	2.5	30	6/4	22.50
76769	2.5	28	6/3	21.20
76770	2.5	33	6/5	24.00
76771	2.5	31	6/4	23.20
76773	2.5	30	6/4	19.80
76743	2.5	21	0/8	0.46
76744	2.5	25	0/9	0.54
76745	2.5	28	0/10	0.55
80506	2.7	36	7/5	27.5
80507	2.7	31	7/5	21.2
80537	2.7	36	7/5	24.0
80539	2.7	39	7/5	36.4**
80541	2.7	32	7/5	23.6
80542	2.7	40	7/5	24.6
80543	2.7	32	7/5	20.5
80544	2.7	36	7/5	25.3

* T beams contain 2% tritium and 98% deuterium (i.e. trace tritium).

** Alpha loss evaluated during 3.7–3.75 s near the neutron peak (all other shots are evaluated during 3.4–3.7 s).

- (c) An alpha heating experiment at $I = 1.8$ MA and ≈ 20 –25 MW of 50/50 ‘full DT’;
 (d) Fusion power experiments at $I = 2.0, 2.5$ and 2.7 MA with up to 40 MW of full DT [5, 6].

One of these discharges had the highest sustained fusion power and alpha pressure of any DT shot to date; the alpha parameters as calculated by TRANSP for this shot (No. 76770) are summarized in Table II. One of these discharges also had the highest instantaneous fusion power to date, i.e. 10.7 MW (No. 80539).

At the higher plasma currents $I \geq 1.8$ MA, the radial profiles of the magnetic safety factor $q(r)$ and the fusion reaction rate $S(r)$ are important in determining the local first orbit loss rate (see Section 3). For the first orbit loss calculations in this paper, the $q(r)$ and $S(r)$ profiles were taken from time dependent TRANSP simulations, rather than from direct measurements, since these profiles were measured on only the subset of the shots for which lost alpha data were available. However, the TRANSP profiles generally agreed well with the $q(r)$ measurements from MSE and $S(r)$ measurements from the neutron collimator, as described in Appendix B.

4.2. Lost alpha signals and backgrounds

Data on alpha loss was obtained for all of the discharges in the initial DT run of December 1993. The raw scintillator image data from two of the first DT shots at $I = 0.6$ MA and $I = 2.0$ MA are shown in Fig. 3. These data were averaged over the near steady state time 0.4–0.7 s after the start of NBI, i.e. 3.4–3.7 s after the start of the plasma current. The $I = 0.6$ MA shot had 5 MW of NBI (50/50 D/T), while the $I = 2.0$ MA shot had 29 MW of NBI (40/60 D/T). The latter was the discharge with the maximum fusion power of 6.2 MW during the initial DT run period at $I = 2.0$ MA [5, 6].

The height co-ordinate in these 3-D plots is proportional to the signal intensity as measured by the CCD camera, the output of which is linear with light intensity over the range from ≈ 45 units (black level) to ≥ 200 units (out of 256). The elevated square region covering most of the pixel versus line plane corresponds to the quartz fibreoptic bundle, which emits visible light in the same wavelength range as the scintillator ($\approx 550 \pm 35$ nm), owing to the neutron and gamma induced fluorescence [10, 18]. The lost alpha signals are the localized peaks within this background. It is immediately clear that the alpha signal/neutron background ratio is larger for the $I = 0.6$ MA case than for the $I = 2.0$ MA case, directly indicating a larger alpha collection fraction at the lower current, as expected.

TABLE II. ALPHA PARTICLE PARAMETERS CALCULATED BY TRANSP FOR SHOT No. 76770

Major radius	2.52 m
Minor radius	0.87 m
Plasma current	2.5 MA
NBI power	33 MW
Fusion power	7.5 MW
Alpha power	1.5 MW
$\langle \beta \rangle$	1.01%
$\langle \beta \alpha \rangle$	0.03%
$\beta_\alpha(0)$	0.27%
$\beta(0)$	3%
$R \nabla \beta_\alpha$	0.02
W_{tot}	6.2 MJ
W_α	0.2 MJ
$V_\alpha/V_A(0)$	1.6
$n_\alpha(0)/n_e(0)$	0.3%
First orbit loss fraction	$\approx 3\%$

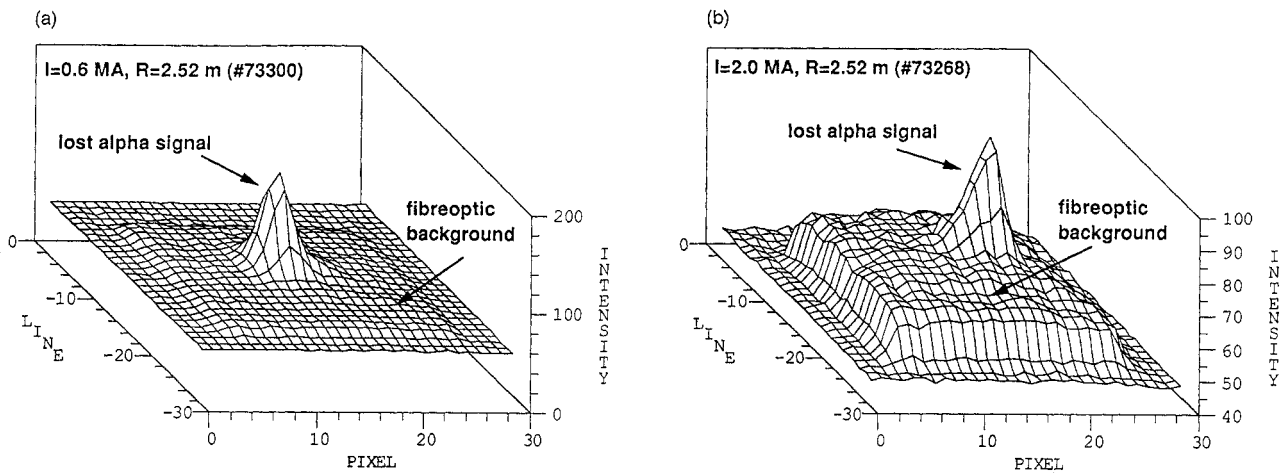


FIG. 3. Raw data of the scintillator light emission patterns in the 90° detector at (a) $I = 0.6$ MA and (b) $I = 2.0$ MA. The raised square region corresponds to the neutron/gamma background light produced in the quartz fiberoptic bundle. The localized peaks correspond to the alpha loss signals. These images are averaged over 0.4 to 0.7 s after the start of NBI for discharges with a $\approx 50/50$ DT mix.

These raw CCD images are interpreted using the scintillator ‘map’ shown in Fig. 4. The grid of pitch angle versus gyroradius co-ordinates was calculated for incident alpha particles using a detector simulation code [14], which includes the energy attenuation in the 3 μm aluminium foil (typically $\approx 20\%$ at 3.5 MeV, with a cut-off at ≈ 1 MeV) and the geometrical spread allowed by the finite aperture sizes. The scintillator position with respect to the quartz bundle was determined by an in-vessel calibration before the DT run [10]. Note that these grid points represent only the centroids of the impact patterns for alphas of a given pitch angle and gyroradius; however, the full impact distribution and the optical resolutions are taken into account in interpreting the pitch angle and gyroradius distributions (Sections 4.7 and 4.8).

These camera data are analysed by subtracting the brightness of the background region of the image from the image as a whole. The background subtraction region was within the boundary of the scintillator image, but outside the region of the alpha signal, as indicated by the gray region in Fig. 4. The image was then unfolded using the scintillator map of Fig. 4 into pitch angle versus gyroradius centroid (χ, ρ) distributions, such as shown in Fig. 5 for the data of Fig. 3. The total lost alpha signal level is found by integrating over the (χ, ρ) co-ordinates shown in Fig. 4, i.e. $\chi = 45\text{--}90^\circ$ and $r = 3.5\text{--}10$ cm, which includes essentially all of the lost alpha signal for all of the plasma currents, and then subtracting out the level in the background region separately for each time frame.

The signal levels in the background region of the camera field scaled linearly with the standard neutron

rate monitors when integrated over 0.4–0.7 s after the start of NBI (within $\approx 10\%$), as expected from independent measurements of the fiberoptic fluorescence [18]. The time dependence of the signal level within the whole (χ, ρ) map of Fig. 4 was simultaneously

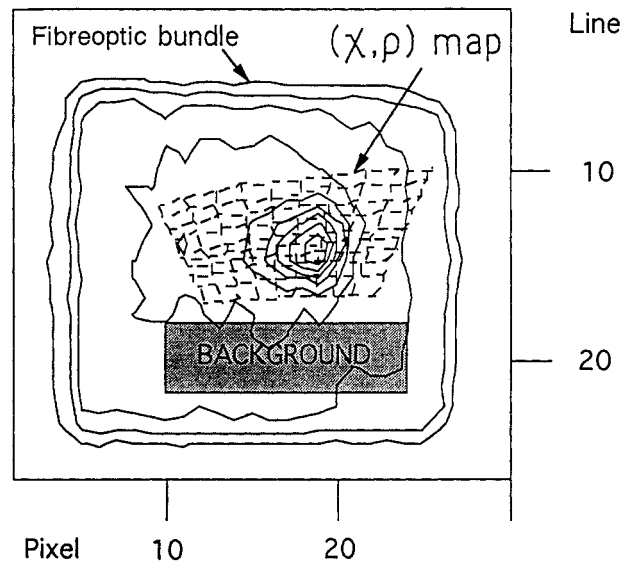


FIG. 4. A map of the 90° detector’s scintillator plane showing the lost alpha data for the $I = 2.0$ MA shot of Fig. 3, along with the pitch angle (χ) versus gyroradius (ρ) co-ordinate system used to interpret it. These co-ordinates are the centroids of the impact positions of ions passing through the entrance apertures at a given χ and ρ . The pitch angle co-ordinate runs from 90 to 45° from left to right in 5° increments, and the gyroradius co-ordinate runs from 6 to 10 cm in 1 cm intervals from bottom to top. The shaded region within the fiberoptic bundle is used for neutron background subtraction.

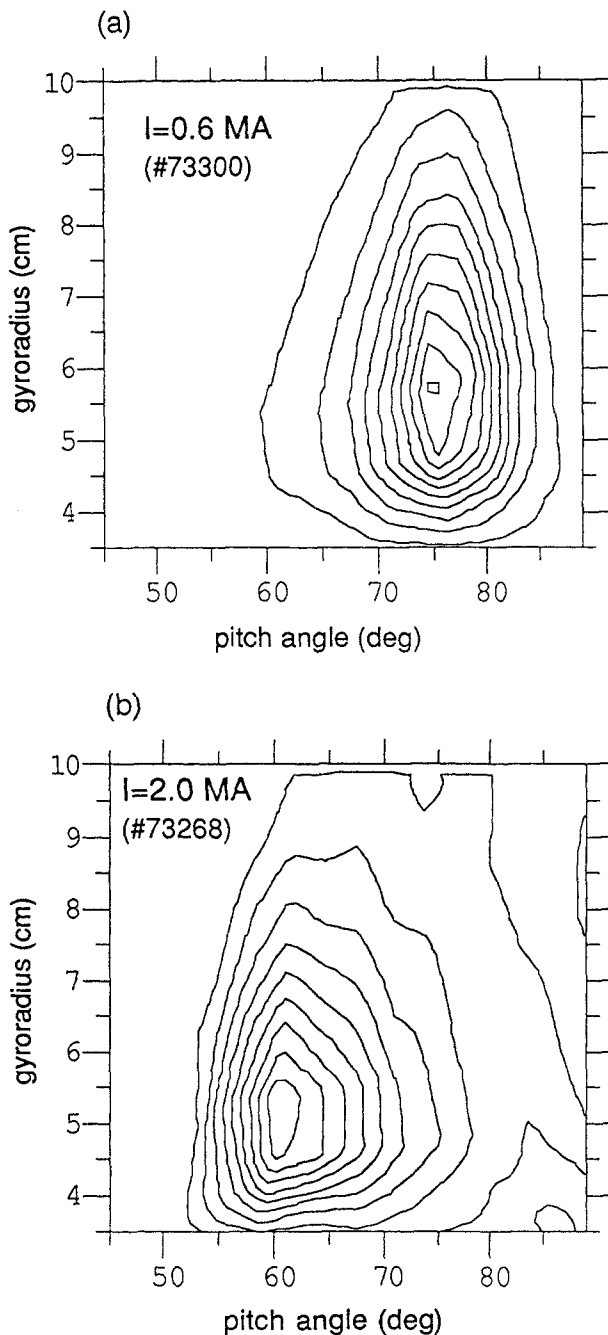


FIG. 5. Unfolded scintillator images for the data of Fig. 3. The background has been subtracted out, and the light intensity plotted using the pitch angle and gyroradius map shown in Fig. 4. The contours are drawn in steps of 10% of the maximum signal level.

monitored using a photomultiplier tube, and for high current discharges it closely followed the neutron rate versus time. This was expected since at high currents $\approx 3/4$ of the total signal within the whole map was due to the neutron background (see Fig. 3).

However, the background signal level as determined from the camera images had an instrumental delay of ≈ 50 – 100 ms with respect to the standard neutron signals (a similar delay was seen in the camera's response to an optical test pulse anywhere in the field of view). For the data in this paper the time dependence of the alpha loss signal was not explicitly corrected for this delay, but instead the time dependence of the alpha loss signal was compared with the time dependence of the fiberoptic neutron background signal (within the gray area of Fig. 4). This procedure automatically corrects for this hardware delay and ensures accurate cross-timing between the alpha loss and the neutron signals.

The time dependence of the net alpha loss signal for a typical DT discharge is compared with that for an equivalent DD discharge in Fig. 6. Both these discharges had $I = 2.0$ MA and 27 MW of NBI between 3.0 and 3.7 s (Nos 73 235, 73 236), and the lost alpha detector camera gains and data analysis procedures were exactly the same for both. The total loss signal within the (χ, ρ) grid during the DD shot was $< 5\%$ of the signal during the DT shot (after the appropriate background subtractions); therefore essentially all of the signal during the DT shot was due to alpha particle loss, and not to DD fusion product loss.

The magnitude of the DT alpha loss cannot be directly compared with the DD fusion product loss since the scintillator light output from 1 MeV tritons has not been directly measured [9, 10]. However, at $I = 0.6$ MA, where the DT and DD fusion product loss fractions should be similar, the measured scintillator light output *per neutron* for DT versus DD discharges

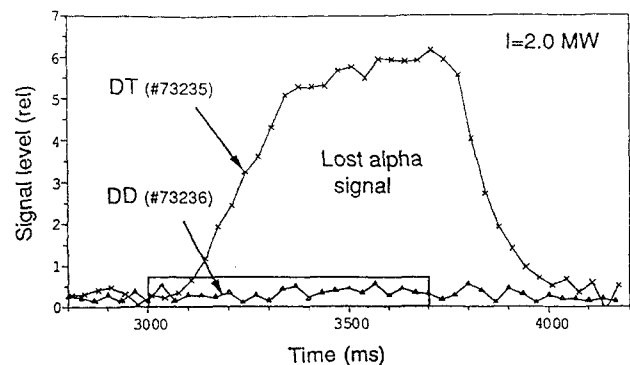


FIG. 6. Time dependences of the net alpha loss signals for comparable DT and DD discharges, both at $I = 2.0$ MA and 26 MW of NBI over 3 to 4 s. These signals were integrated over the (χ, ρ) map of Fig. 4, and the neutron background was subtracted out. The DD signals were $\leq 5\%$ of those during DT, and so are negligible in the analysis of the DT discharges.

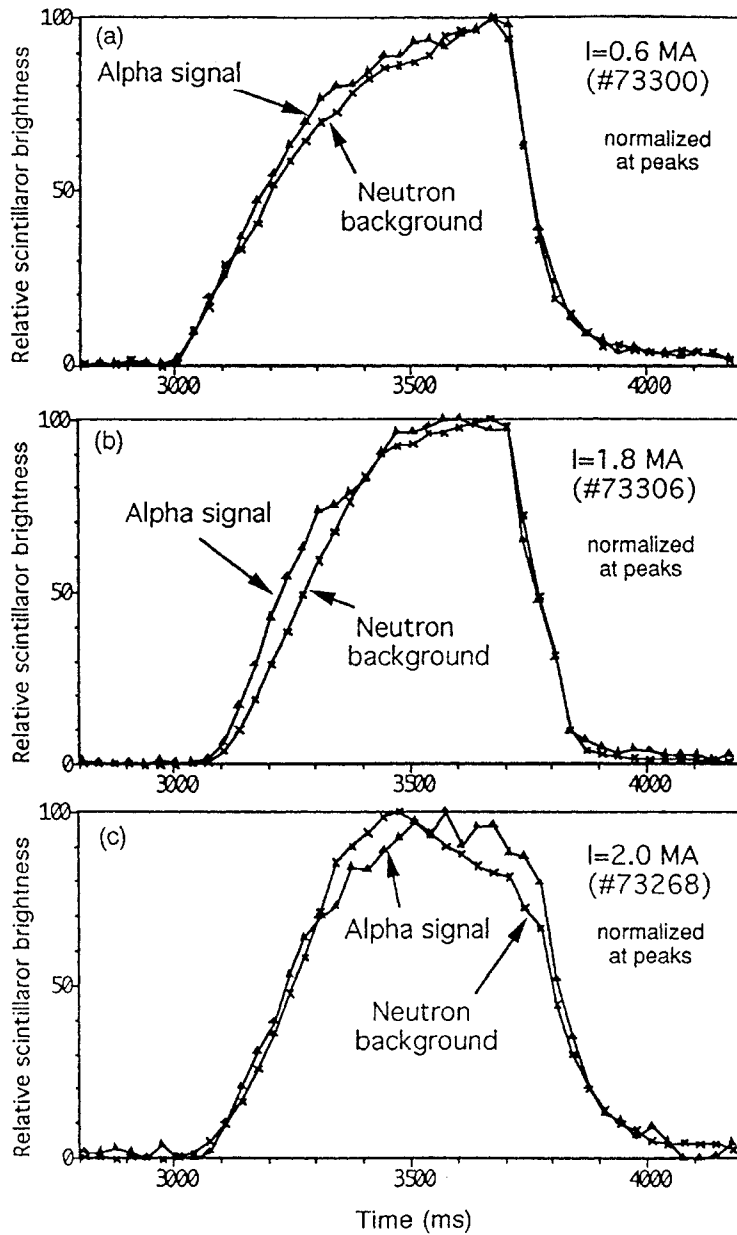


FIG. 7. Time dependences of the lost alpha signals and neutron background levels for DT discharges at (a) $I = 0.6 \text{ MA}$, (b) $I = 1.8 \text{ MA}$ and (c) $I = 2.0 \text{ MA}$. These signals are normalized to each other at their peak values. The neutron background is due to the fiberoptic fluorescence, which is proportional to the DT neutron rate. The alpha loss signal follows fairly closely the DT neutron signal versus time.

was $\approx 1.5 \pm 0.3$, i.e. the signal levels during DT were ≈ 100 times larger than during similar DD discharges, mainly due to the ≈ 60 times larger neutron flux in DT. This is roughly consistent with the expected light output ratio, since only a fraction of the 3 MeV proton energy is deposited within these thin P46 scintillators. Thus, the measured alpha loss signal was close to that expected from the previous DD measurements. The absolute calibration for DT is discussed in Section 4.6.

4.3. Time dependence

In Fig. 7 the time dependence of the lost alpha signal is compared with the time dependence of the neutron background signal for three typical DT shots. The alpha loss signals are the averages within the (χ, ρ) grid of Fig. 4, after subtraction of the neutron induced fiberoptic background level (gray area of Fig. 4). The 'neutron background' traces in Fig. 7

are the signal levels within the 'gray area' shown in Fig. 4, which are dominated by the fiberoptic fluorescence, which can be assumed to be proportional to the DT neutron rate (see Section 4.2). These two signals are normalized to each other at their peaks to show their relative time behaviour more clearly.

The total alpha loss rate for the single source tritium shot at $I = 0.6$ MA followed closely the neutron rate versus time, as it did for all other low to moderate powered low current DT shots ($I \leq 1.4$ MA). However, for the moderate powered single tritium source shot at $I = 1.8$ MA, and for the high powered full DT shot at $I = 2.0$ MA (which was the discharge with the maximum fusion power at this current), there were some differences between the time dependences of the alpha loss and neutron background signals during and after NBI.

These differences are shown more clearly in Fig. 8, which compares the time dependence of the alpha loss signal normalized by the neutron background signal to the time dependence of the calculated first orbit alpha collection rate for the discharges of Fig. 7. These calculated alpha collection rates were based on TRANSP analyses of the profile shapes versus time, and were normalized to the relative alpha loss per neutron data at 0.6 s after the start of NBI. For all cases the time dependence of the normalized alpha loss was within about $\pm 20\%$ of the calculated first orbit loss rate. However, given the estimated experimental uncertainty (shown by the error bars), it is not possible to isolate any real discrepancies between the data and the model. The uncertainties are discussed in more detail in Section 4.6.

The conclusion from these and the other DT discharges of Table I is that the time dependence of the alpha loss signals is roughly consistent with the expected prompt first orbit loss, i.e. approximately proportional to the DT neutron rate during a single discharge at a constant current. There was no sign of any significant MHD induced losses during these DT discharges, such as was previously seen in DD as a sudden increase in the ratio of the fusion product loss to the neutron rate (see Section 6.3). There was also no sign of the 'delayed loss' seen previously in DD (see Section 4.9).

4.4. Neutron rate dependence

Any systematic increase in the alpha loss rate with increasing DT fusion power could indicate some new 'collective' alpha loss mechanism, since the confined alpha population presumably causing such an effect

should increase with the DT reaction rate. This dependence of the alpha loss on the neutron rate should be examined at a constant plasma current, since then the 'single particle' first orbit alpha loss rate should be nearly independent of the DT neutron rate.

Figure 9 shows the neutron normalized alpha loss to the 90° detector versus the peak DT fusion power for all of the high current $I \geq 2$ MA discharges in the data set of Table I. The alpha loss was averaged over the near steady state period 0.4–0.7 s after the start of NBI, and was normalized to the standard neutron rate signals integrated over that time. The resulting alpha loss rates per DT neutron were further normalized to the calculated 'alpha collection fraction' for the 90° detector at $I = 0.6$ MA, as explained in Section 4.5 below. This also allows the expected first orbit alpha loss levels to be shown in Fig. 9.

The result was that there was *no* significant increase in the lost alpha collection fraction with increasing DT fusion power at a given plasma current up to the maximum of 10.7 MW, which corresponded to ≈ 2 MW of alpha source power. At $I = 2.0$ MA the range of DT neutron rates covered a factor of ≈ 40 , where the lowest alpha source rates came from 2% tritium shots, with DT rates similar to their DD neutron rate (the contribution from DD fusion product loss was subtracted out for these cases). The alpha loss in the $I = 2.7$ MA discharge with the highest DT rate of 3.6×10^{18} n/s was evaluated near the peak of its fusion power (3.7–3.75 s), instead of averaged over 0.4–0.7 s after the start of NBI, since the neutron rate changed significantly versus time during this shot. The calculated first orbit alpha collection fraction at the time of maximum neutron rate was 3.1×10^{-9} , which was $\approx 30\%$ above the measured value for this discharge.

The conclusion from this analysis is that the measured alpha collection fraction did not show any signs of collective alpha loss with increased DT rate, and that the results were approximately consistent with the expected first orbit loss, given the uncertainties discussed in Section 4.6. Also, the observed shot to shot variations of $\approx 20\%$ in the measured alpha loss rate versus neutron rate were not correlated with the shot to shot variations of ≈ 10 – 15% in the calculated first orbit loss collection fraction around these averaged levels.

4.5. Plasma current dependence

The plasma current dependence of the neutron normalized alpha loss is shown in Fig. 10 for all the DT discharges of Table I. Each cross represents a differ-

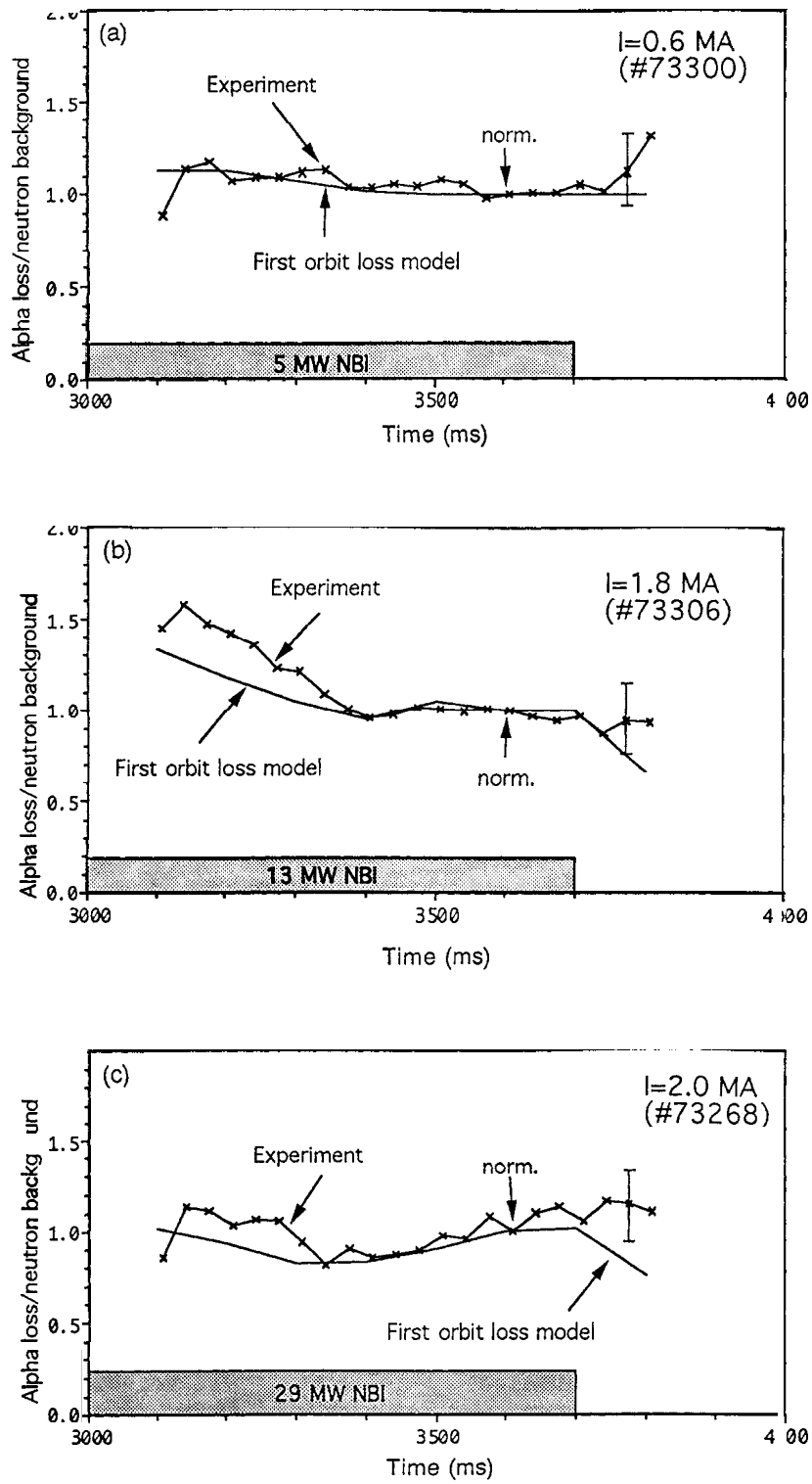


FIG. 8. Time dependence of the neutron normalized alpha loss for the discharges of Fig. 7, along with the time dependence of the calculated first orbit alpha loss for these discharges. These calculations take into account the time evolutions of the plasma current and neutron source profiles, as modelled by the TRANSP code. The calculated first orbit loss fraction is roughly independent of time, i.e. similar to the data. The error bars are an estimate of the experimental uncertainty.

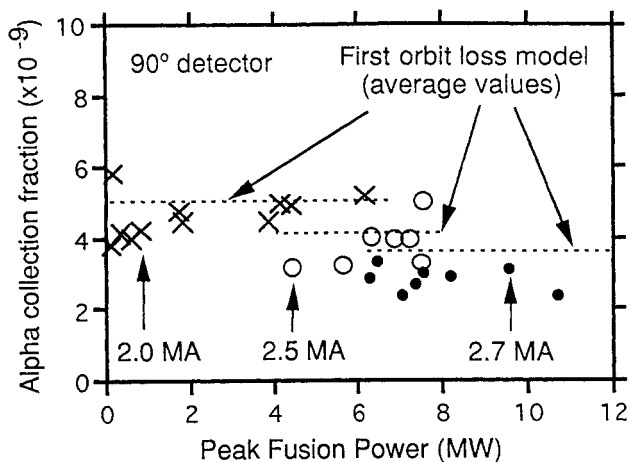


FIG. 9. Alpha particle collection fraction versus the peak fusion power for discharges at $I = 2.0, 2.5$ and 2.7 MA, integrated over 0.4 to 0.7 s after the start of NBI. The alpha collection fraction is the global alpha loss rate into the detector divided by the total neutron rate during this time (normalized as discussed in Section 4.5). At a given plasma current, the alpha collection fractions are roughly independent of the DT neutron rate, showing the absence of any observable 'collective' alpha loss effect at the highest fusion power. The expected average first orbit loss rates for each of these currents is also shown; the shot to shot variations in the calculated first orbit loss at a given current are typically within $\pm 10\%$ of this average.

ent discharge for which the alpha loss signals are integrated over the (χ, ρ) map of Fig. 4 during the near steady state period 0.4 – 0.7 s after the start of NBI. The neutron background has been subtracted out, as discussed in Section 4.3, and the alpha loss signals have been normalized to the standard neutron rate signals averaged over this time.

This data are further normalized to the *calculated* first orbit alpha collection fraction at $I = 0.6$ MA, where the first orbit loss is expected to dominate over any other loss process. This calculated alpha collection fraction is defined as the first orbit alpha loss rate passing through the detector's apertures onto the scintillator, divided by the total DT neutron (alpha) source rate (see Section 4.3). For example, an $I = 2.0$ MA discharge with $\approx 2 \times 10^{18}$ DT n/s with an alpha collection fraction of $\approx 5 \times 10^{-9}$ would have $\approx 10^{10}$ alphas/s passing through the apertures and hitting the scintillator. This normalization of the data to the first orbit loss calculation at $I = 0.6$ MA provides an in situ calibration of the alpha loss at higher currents (see also Section 4.6).

The result was that the whole DT data set was consistent with the calculation of first orbit alpha loss indicated by the shaded region in Fig. 10. This implies that there was no substantial anomalous alpha particle

loss seen in the 90° detector for this data set. Although the data of Fig. 10 refer to time averaged alpha loss over a 0.3 s interval near the peak of the DT neutron emission, there was also little or no evidence for fluctuating MHD induced alpha particle loss in these discharges.

The first orbit model alpha loss region shown in Fig. 10 is based on the Lorentz code analysis for several discharges at each current (see Section 3). The neutron source and plasma current profiles used for these calculations were taken from the time dependent TRANSP analysis of these discharges at 0.6 s after the start of NBI. Similar analyses made previously using the profiles from the time dependent SNAP transport code gave a somewhat differently shaped model prediction, as shown previously by the lower edge of the shaded region in Fig. 4 of Ref. [5] (the TRANSP based calculations shown by the upper edge of the shaded region in that figure are similar to the TRANSP calculations shown here). The profiles from the TRANSP code are considered to be more accurate, and have been checked against the measured profiles, as discussed in Appendix B.

The scatter in the data at a given plasma current did not show any systematic increase with DT neutron rate, as discussed in the previous section. The largest discrepancy between the data and the first

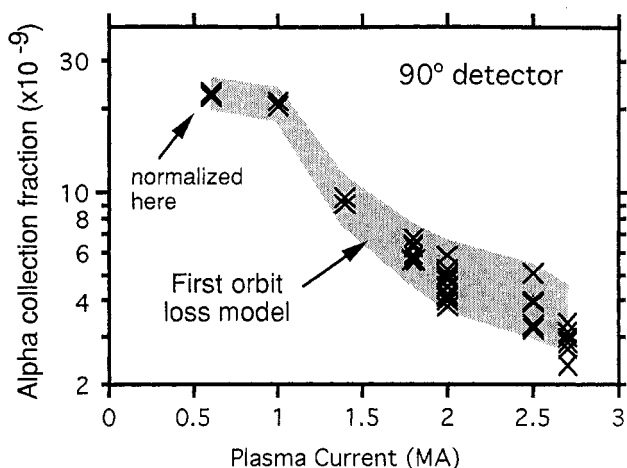


FIG. 10. Dependence of the alpha collection fraction on the plasma current for the whole set of DT discharges (Table I). The data are normalized to the calculated first orbit alpha collection fraction at $I = 0.6$ MA, where the first orbit loss is expected to dominate. All the data fit the first orbit model within the joint uncertainties, which at $I = 2.0$ MA are about $\pm 30\%$ for the modelling and $\pm 30\%$ for the measurements. The relative uncertainties in both the data and the modelling decrease towards lower plasma current where the first orbit loss fraction is largest (see also Appendix A).

orbit loss modelling was at the highest plasma current of $I = 2.7$ MA, where the signal to background ratio was the smallest and the experimental uncertainty was the largest. The uncertainties in the measured and calculated alpha losses are discussed in more detail in Section 4.6. The conclusion from that analysis is that the agreement between experiment and theory at $I \approx 2.0$ MA is good to within a joint uncertainty of about $\pm 50\%$, when based on the in situ calibration at $I = 0.6$ MA.

4.6. Uncertainties and absolute calibration

Figures 8 to 10 showed good agreement between the measured alpha loss in the 90° detector and the calculated first orbit alpha loss. However, there were several uncertainties not shown explicitly in those figures, which are discussed below, along with the absolute calibration.

4.6.1. Uncertainties in the measurements

The measurements of the neutron normalized alpha loss versus plasma current as summarized in Fig. 10 showed a ± 5 – 10% scatter at $I \leq 1.4$ MA, but up to a $\pm 30\%$ scatter at $I = 1.8$ – 2.7 MA. At the higher plasma currents, there were also time variations in the normalized alpha loss of ± 10 – 20% during 0.4–0.7 s after the start of NBI, as shown in Fig. 8. Since there was little or no systematic variation with the DT neutron rate, as shown in Fig. 9, this scatter is most likely caused by a variation in the first orbit loss due to plasma profile changes (see Section 4.6.2), or to uncertainties in the evaluation of the measured alpha loss.

The main experimental uncertainty in these measurements was due to the background subtraction processes (Section 4.2). For example, at a current of $I = 2.0$ MA, the peak signal to neutron background ratio was only about 2.5:1 (see Fig. 3), and the average signal to background level within the whole (ρ, χ) map over which the analysis was made was $\approx 1:3$. Thus, if the average background level within the (ρ, χ) map was only $\approx 10\%$ different from the average level within the ‘background region’ of the scintillator (see Fig. 4), there would be an $\approx 30\%$ systematic error in the inferred alpha signal level at this current. This error cannot be easily evaluated, since the 2-D pattern of the fibreoptic background light cannot be measured without the presence of alpha loss (although it is very likely to be flat, as assumed in the present analysis). This type of error would change the inferred alpha loss collection fraction by some constant number over the

whole range of plasma currents, and so would not significantly change the shape of the inferred alpha loss versus current in Fig. 10.

Other measurement uncertainties include the drift in the camera gain versus time, which was monitored daily and was $< 10\%$ over the duration of these experiments, and a shot to shot uncertainty of $\approx 5\%$ in the epithermal DT neutron measurement used for normalization [19]. The fibreoptic transmission was monitored by a test fibre close to the signal fibres, and showed a negligible change in both transient and permanent opacity over this experimental run. Overall, the neutron normalized alpha loss measurements for the full DT shots at $I \approx 1.8$ – 2.7 MA are uncertain by an estimated $\pm 30\%$ with respect to the alpha loss at $I = 0.6$ MA.

4.6.2. Uncertainties in the calculations

The calculated alpha first orbit collection fraction at 90° for $I = 0.6$ MA had a variation of $\leq 5\%$ over the three DT shots in Table I. At higher currents of $I = 1.8$ – 2.7 MA these variations were ± 10 – 15% , most likely owing to the increased sensitivity to plasma current and neutron source profiles, as discussed in Section 2. These calculations used the profiles from the TRANSP code at 0.6 s after the start of NBI.

The profiles from TRANSP were spot checked with measurements of $q(r)$ and $S(r)$ for some of the discharges in this data set, as described in Appendix B. The 90° alpha collection fractions calculated using the measured $q(r)$ profiles were within $\pm 10\%$ of those using the TRANSP $q(r)$ profiles over $I = 0.6$ – 1.8 MA, and the alpha loss calculated for an $I = 1.8$ MA discharge using the measured neutron profile was within $\approx 15\%$ of that calculated using the TRANSP neutron profile. There was also an ≈ 10 – 20% uncertainty in these calculations due to imprecise knowledge of the three aperture dimensions which determine the alpha flux into the detector. Overall, the calculated first orbit alpha loss at the highest currents $I \geq 1.8$ MA has an estimated uncertainty of $\pm 30\%$.

In summary, the measured alpha loss for high current, high power full DT discharges agreed well with the calculated first orbit alpha loss, when normalized to the reference discharges at $I = 0.6$ MA, which serve as an in situ calibration, given their joint uncertainty of $\leq 50\%$ (i.e. $\pm 30\%$ each from experiment and calculation). This is approximately the same uncertainty found previously in comparing measured and calculated losses for DD fusion products in the 90° detector [11].

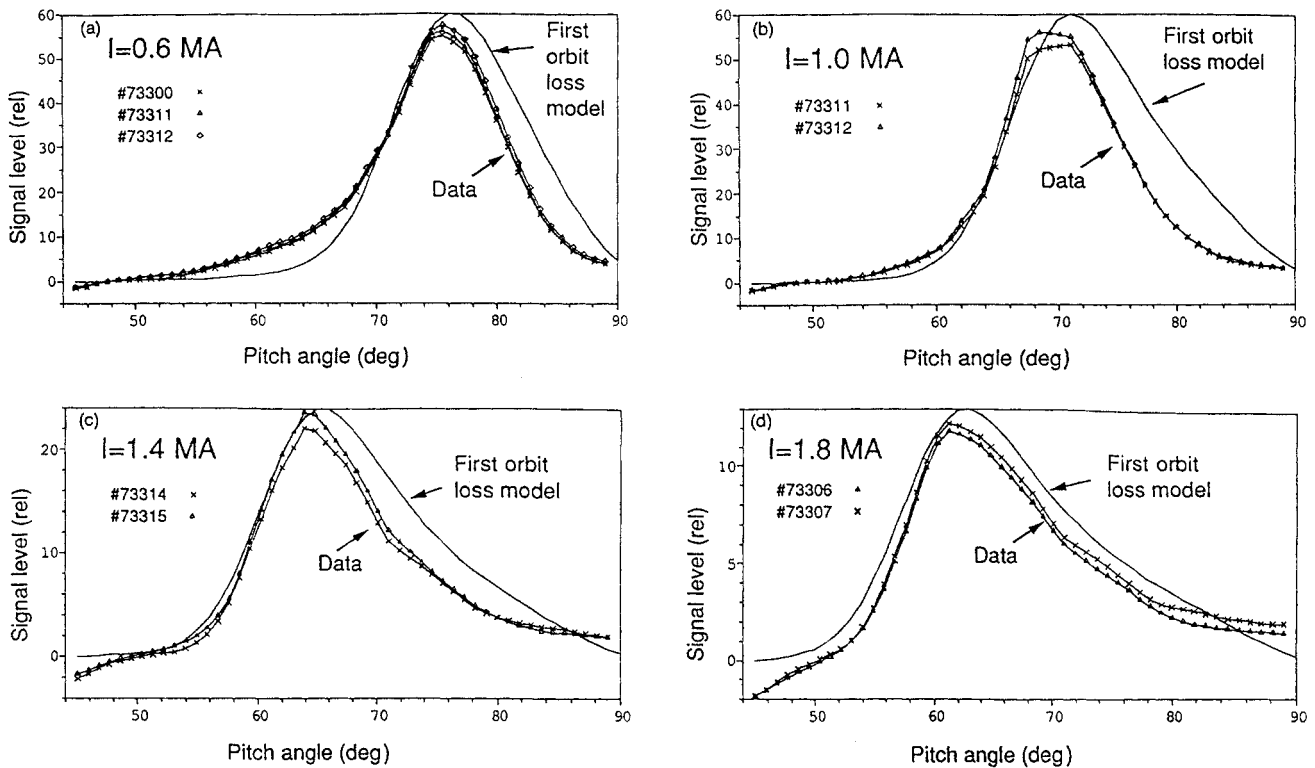


FIG. 11. Pitch angle distributions of the alpha loss at $I = 0.6$ – 1.8 MA for single tritium source discharges. These distributions agree fairly well with the first orbit loss calculation made using the TRANSP profiles, which were corrected for the geometric and optical resolutions of the detectors. The measured and calculated curves are normalized vertically to each other near their peaks, but the horizontal axis was absolutely calibrated by an in-vessel alignment to within $\approx 3^\circ$.

4.6.3. Absolute calibration

An independent absolute calibration of the total lost alpha flux onto the scintillator was made by exposing a sample P46 scintillator to a beam of 3.5 MeV alphas at the Los Alamos Van de Graaff accelerator [9, 10]. The scintillator light due to an absolutely calibrated alpha beam was compared with the light from a portable calibration lamp, which was then transferred into the TFTR vessel and mounted at the scintillator locations during a machine opening.

The absolute alpha collection fraction estimated in this way for the $I = 0.6$ MA discharges was $\approx 1.4 \times 10^{-8}$, which was close to the calculated alpha collection fraction of $\approx 2.2 \times 10^{-8}$ [10]. The absolute calibration was estimated to have a $\approx 60\%$ uncertainty, i.e. $\approx 50\%$ from the measurements at the Van de Graaff accelerator, and $\approx 25\%$ from the calibration lamp. Thus, the measured alpha loss in TFTR agreed with the absolute calibration to within their joint uncertainties. The data of Figs 9 and 10 were normalized to the calculated first orbit loss at $I = 0.6$ MA owing to the relatively large uncertainty in this absolute calibration.

4.7. Pitch angle dependence

The first orbit loss model predicts that the alpha loss should be peaked near the pitch angle of the 'fattest' banana orbit, which passes closest to the high source rate region near the plasma centre. This pitch angle should also decrease systematically with increased plasma current, as illustrated in Fig. 2. Unexpected changes in these pitch angle distributions have previously been associated with anomalous loss of DD fusion products; for example, the 'delayed loss' was seen at an unusually high pitch angle [12], and MHD induced loss was sometimes localized near the passing/trapped boundary [16].

The pitch angle distributions of alpha loss in the single tritium source shots in the plasma current range $I = 0.6$ – 1.8 MA are shown in Fig. 11. The shapes of these distributions are quite reproducible from shot to shot, and agree well with those calculated from the first orbit loss code. The model curves shown take account of the $\approx 5^\circ$ optical resolution and $\approx 3^\circ$ geometrical resolution of the detector system, and the measurements were absolutely calibrated with respect to

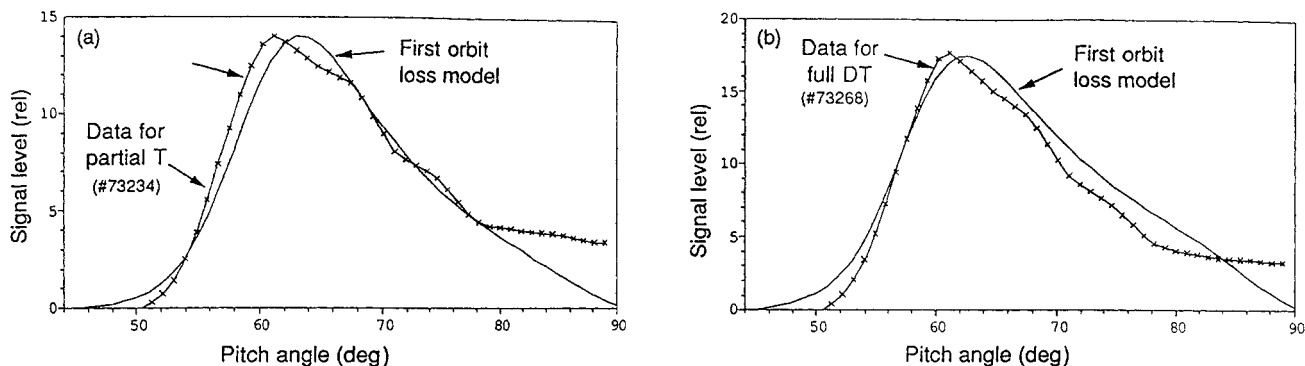


FIG. 12. Pitch angle distributions of alpha loss for two DT discharges at $I = 2.0$ MA: (a) with a single tritium source (No. 73234) and (b) with full DT (No. 73268). There is no significant difference between the pitch angle distributions for these two cases, indicating the absence of any new alpha loss process at high power in DT. Both distributions agree well with the calculated shape of the first orbit loss distribution. The measured and calculated curves are normalized vertically to each other near their peaks, but there the horizontal axis was absolutely calibrated by an in-vessel alignment to within $\approx 3^\circ$.

pitch angle by in-vessel alignments to within $\approx 3^\circ$. The modelling does not account for the geometrical cut-off in the pitch distribution above $\approx 83^\circ$, so tends to over-estimate the loss at high pitch angles at the lowest plasma currents.

The pitch angle distributions of the measured alpha loss for two of the higher current $I = 2.0$ MA shots are shown in Fig. 12. One of these shots was a single tritium source shot with a relatively low DT reaction rate (No. 73234), and the other was the shot with the maximum fusion power of 6.2 MW at $I = 2.0$ MA (No. 73268). The measured and calculated pitch angle distributions are similar to each other and to the first orbit model calculations, indicating the absence of any new alpha loss mechanism in the discharge with the highest confined alpha population at this current.

4.8. Gyroradius dependence

The first orbit loss model predicts that alphas will be lost near their birth energy of ≈ 3.5 MeV, with a Doppler spread of up to about ± 0.5 MeV caused by the beam-target and beam-beam reactions (which contribute $\approx 75\%$ to the fusion reactivity). The alpha loss orbits and loss fractions do not change significantly within this energy range, so the alpha orbits in this paper were calculated by assuming an alpha energy of exactly 3.5 MeV (in alpha confinement terms, the maximum spread of ± 0.5 MeV is equivalent to only a $\pm 7\%$ change in plasma current).

The gyroradius distributions of the measured alpha loss for the single tritium source shots in the current scan from $I = 0.6$ – 1.8 MA are shown in Fig. 13. These distributions are plotted versus the gyroradius centroid co-ordinate along the scintillator map shown in

Fig. 4. There is a considerable spread in this direction due to the finite aperture sizes and optical resolutions, so that a monoenergetic 3.5 MeV alpha distribution is not expected to be well localized at its corresponding $\rho = 5.4$ cm for these cases. The modelled gyroradius distributions for 3.5 MeV alphas are also shown in Fig. 13, including these spreads as calculated by the detector simulation code. The shapes of the experimental distributions are quite reproducible and agree fairly well with the model for 3.5 MeV alpha loss. The small differences at large and small ρ are most likely due to uncertainties in the background subtraction or modelling. Note that the measured distributions were absolutely calibrated by an in-vessel alignment to within ≈ 1 cm in this gyroradius centroid co-ordinate.

The gyroradius distributions of the measured alpha loss for two of the $I = 2.0$ MA shots are shown in Fig. 14. One of these shots was a single tritium source shot with a relatively low DT reaction rate (No. 73234) and the other was the shot with the maximum fusion reactivity at this current (No. 73268). The measured gyroradius distributions are similar to each other, and are fairly well fitted by the 3.5 MeV alpha loss model. The model curves for 2.5 and 4.5 MeV alphas are also shown for comparison, normalized to a fixed peak height.

The conclusion from this analysis is that the energy distribution of the measured alpha loss in the 90° detector is independent of the DT reaction rate, and roughly consistent with the expected first orbit loss distribution (i.e. at gyroradii corresponding to alphas at 3.5 ± 0.5 MeV). These gyroradius distributions are also independent of time, similar to those for previous DD fusion product measurements [11].

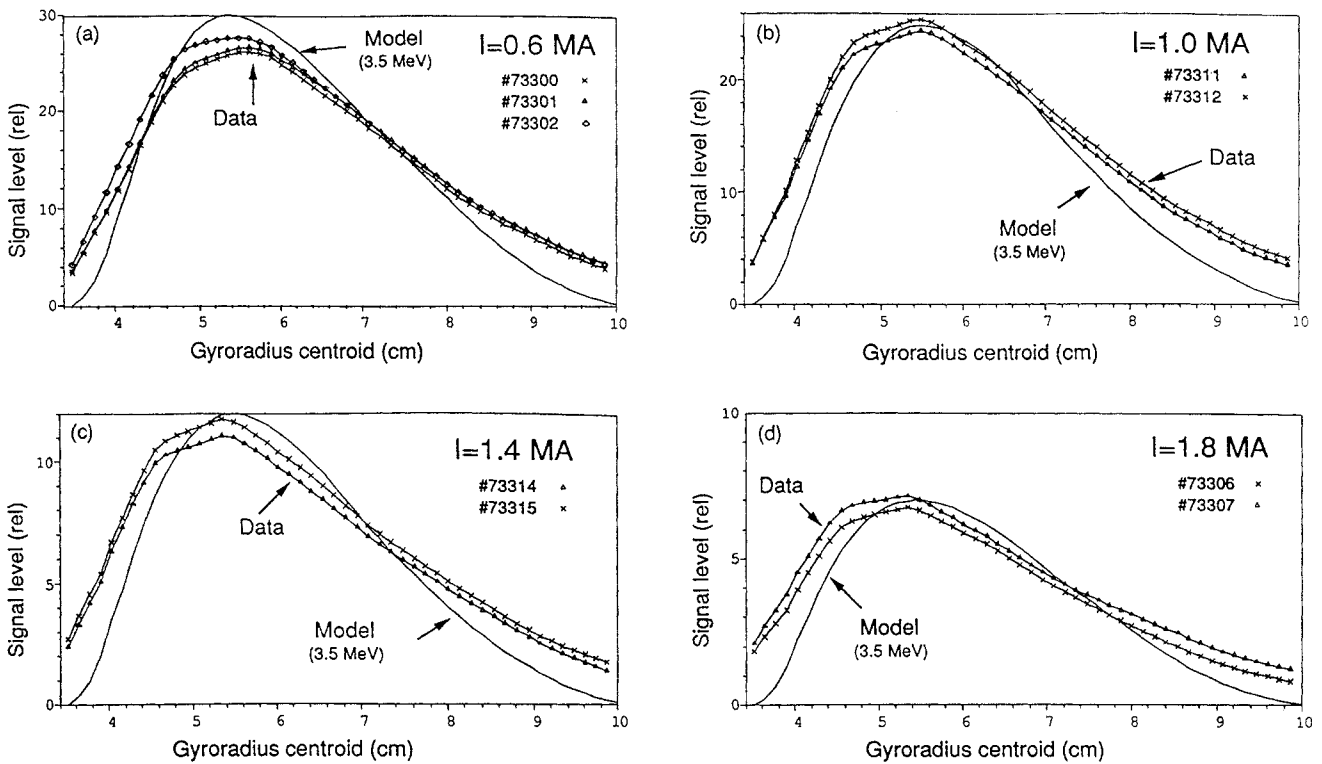


FIG. 13. Gyroradius distributions of alpha loss at $I = 0.6\text{--}1.8$ MA for single tritium source discharges. In all cases these distributions agree fairly well with the model calculations for first orbit alpha loss for 3.5 MeV alphas, after correcting for the geometric and optical resolutions of the detectors. The measured and calculated curves are normalized vertically to each other near their peaks, but the horizontal axes were absolutely calibrated by an in-vessel alignment to within ≈ 1 cm on this scale. The systematic differences between the measured and modelled curves at low and high gyroradii are most likely due to experimental or modelling uncertainties.

However, the presence of a comparable level of lower energy alpha loss components, e.g. at ≈ 2 MeV, cannot be excluded, given the present uncertainties in the modelling and data. Also, it should be noted that the presence of alpha loss at energies below ≈ 1 MeV cannot be determined at all from this detector, owing to the presence of the foil behind the slit aperture of this detector (see Section 2).

4.9. Comparison with DD fusion product loss

The loss of DD fusion products in TFTR (3 MeV protons and 1 MeV tritons) has previously been analysed only for plasmas with $R = 2.62$ m and $R = 2.45$ m. For MHD-quiet plasmas at $R = 2.6$ m the loss at the 90° detector was consistent with first orbit loss [11], but there was an additional delayed loss present at $R = 2.45$ m [16]. The DT discharges described in this paper had a different major radius of $R = 2.52$ m (to optimize performance); therefore, the corresponding DD discharges will be described here explicitly. At least one DD comparison shot was made

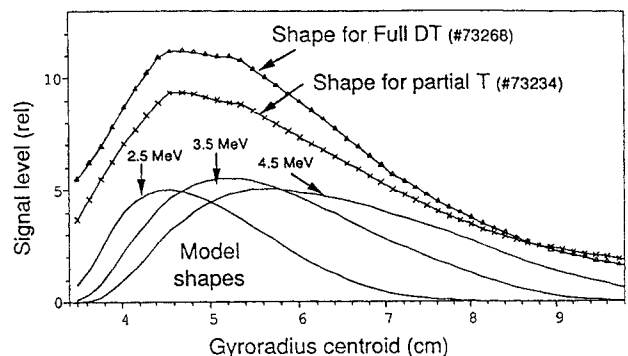


FIG. 14. Gyroradius distributions of alpha loss for two discharges at $I = 2.0$ MA, one with a single tritium source (No. 73234) and the other a full DT discharge (No. 73268). There is no significant difference in the measured distributions for these two cases. Model calculations are shown for three different monoenergetic alpha particle energies, the best agreement being with the 3.5 MeV model curve, as expected for first orbit alpha loss. Note that the toroidal field was 5% higher than that for the discharges in Fig. 13, causing a slight decrease in the gyroradius. The measured and calculated curves are normalized vertically to each other near their peaks, but there the horizontal axis was absolutely calibrated by an in-vessel alignment to within ≈ 1 cm on this scale.

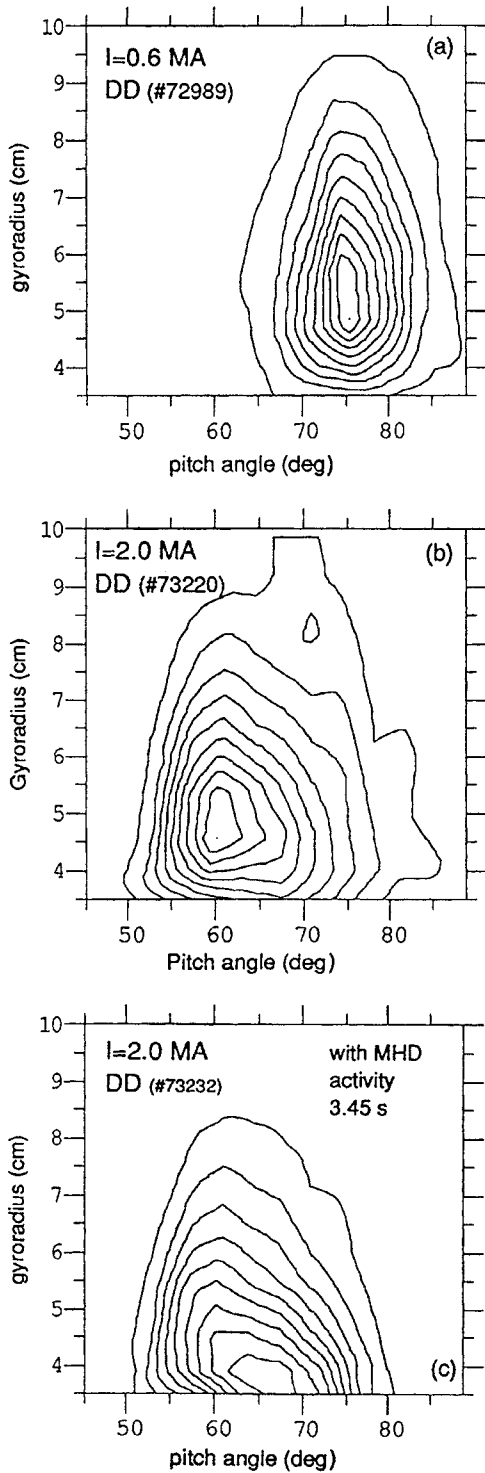


FIG. 15. Pitch angle versus gyroradius distributions for DD fusion product loss at (a) $I = 0.6$ MA and (b, c) $I = 2.0$ MA. These distributions are similar to those for similar DT discharges (as shown in Fig. 5), except for the presence of a small anomalous 'delayed' loss component at high pitch angles ($\chi = 70^\circ$) and low gyroradius ($\rho = 4$ cm) at $I = 2.0$ MA, which was not present in the comparable DT shot. The strength of this anomalous delayed loss feature in DD can increase substantially during MHD activity, as shown in case (c).

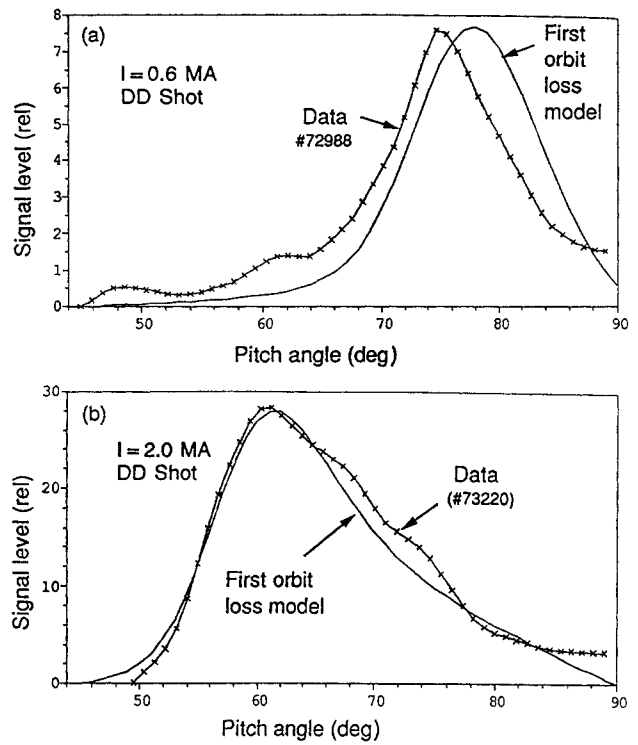


FIG. 16. Pitch angle distributions for DD fusion product loss at (a) $I = 0.6$ MA and (b) $I = 2.0$ MA. The shapes of the measured distributions were similar to those for the DT discharges of Figs 14 and 15, as expected from the first orbit loss model, except for the presence of a small delayed loss component in the data at $\chi \approx 70^\circ$ in DD.

prior to each full DT discharge to avoid DT contamination, as listed in Table I (except at $I = 2.7$ MA).

The patterns of pitch angle versus gyroradius for DD fusion product loss patterns at 90° are shown in Fig. 15 for $I = 0.6$ MA and $I = 2.0$ MA discharges, analysed similarly to the corresponding DT cases in Fig. 5. The DD patterns are basically similar to those for DT. The DD pitch angle distributions as shown in Fig. 16 also agree well with the calculated first orbit loss distribution, which is not expected to vary significantly between DD and DT fusion products. The DD gyroradius distributions shown in Fig. 17 have a small but systematic downward shift in the gyroradius distribution compared with similar DT discharges, which is consistent with the expected $\approx 10\%$ smaller gyroradius of DD fusion products compared with DT alphas.

The largest difference between the DD and DT fusion product losses in the 90° detector was a somewhat larger loss at high pitch and low gyroradius for high current DD cases. This is shown in Fig. 15 for DD, to be compared with Fig. 5 for DT, and also in the DD pitch and gyroradius distributions of Figs 16 and 17. This difference was due to the 'delayed loss'

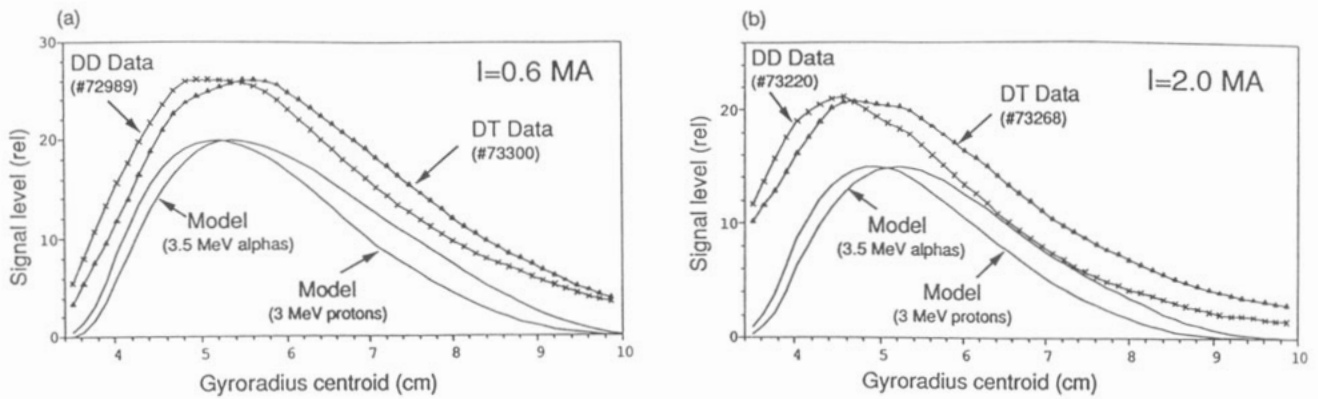


FIG. 17. Gyroradius distributions for DD fusion product loss at (a) $I = 0.6$ MA and (b) $I = 2.0$ MA. The distributions for DD fusion products were peaked at a slightly smaller gyroradius than those for DT, as expected from the first orbit loss model. The discharges at $I = 2.0$ MA also had a $\approx 5\%$ higher toroidal field than those at $I = 0.6$ MA, which also reduced the gyroradius by about this fraction, as expected.

component in DD, similar to that described previously [12, 13, 16], which was significantly reduced or absent in DT. A stronger indication of the absence of delayed loss in DT was seen in $I = 2.5$ MA discharges, as discussed in Section 6.2. This difference between DD and DT may be due to the differing collisional loss between 1 MeV tritons and 3.5 MeV alphas.

The total neutron normalized DD fusion product loss versus plasma current is shown in Fig. 18, analysed similarly to the DT data in Fig. 10. The loss during DD decreases about as expected from the first orbit loss model, as it did for the DT cases. The signal levels per neutron for DT were ≈ 1.5 times larger than those for DD, which was roughly consistent with the expected scintillator response to the respective fusion products (see Section 4.2).

Not shown explicitly in Fig. 18 are the DD discharges with MHD induced fusion product loss, such as that illustrated at the bottom of Fig. 15, where there was a sudden factor of 2 increase in the DD fusion product loss coincident with a minor disruption at 3.45 s. This MHD induced loss is characterized by an increase in the loss at low ρ and high χ , as seen previously [12, 16]. One example of MHD induced loss in DT is discussed in Section 6.3.

5. ALPHA LOSS AT OTHER POLOIDAL ANGLES

Alpha loss was also measured for all of the DT discharges of Table I using similar alpha loss detectors at 60 and 45° below the outboard midplane, and for some of these discharges using a similar but movable detector at 20°, with its aperture placed 1.7 cm radially

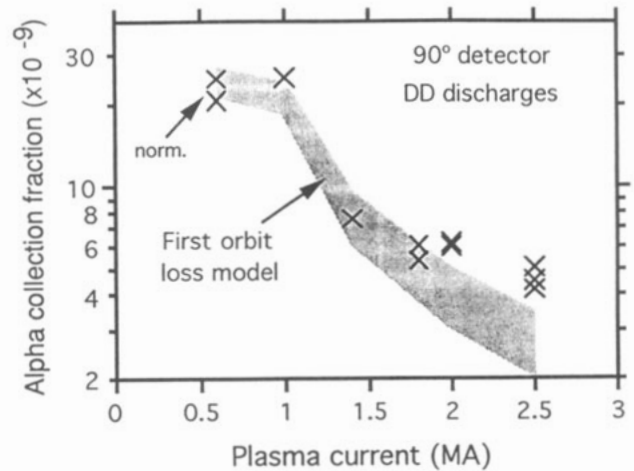


FIG. 18. Dependence of the neutron normalized DD fusion product loss on plasma current, analogous to the DT data in Fig. 10. The data are normalized to the calculated first orbit alpha collection fraction at $I = 0.6$ MA, where first orbit loss is expected to dominate. The data fit the first orbit model for $I \leq 1.8$ MA, but the presence of an additional delayed loss component can be seen at $I \geq 2.0$ MA. These data points represent all the DD shots in Table I.

outside the limiter radius. These results are significant since the neutral beam losses due to TAE modes in DIII-D were concentrated near the outboard midplane [20], and since the TAE induced alpha losses seen in numerical simulations were mainly localized just below the outboard midplane [21].

The alpha loss per neutron at these other three detectors was roughly constant with increasing DT neutron rate at a given plasma current, as it was for the 90° detector data. For example, during a

fusion power scan at $I = 1.8$ MA (similar to those of Fig. 9), the alpha collection fraction in the 90° detector remained constant to within 20% as the DT rate increased between 0.3×10^{18} and 1.3×10^{18} n/s, while the alpha collection fraction in the 20° detector decreased by $\approx 30\%$, and the alpha collection fractions in the 45° and 60° detectors increased by $\approx 30\%$ and $\approx 50\%$, respectively (the latter being subject to the largest measurement uncertainties). The absence of any significant systematic increase in alpha loss with increasing DT neutron rate in these other detectors reinforces the conclusion that there were no ‘collective’ alpha loss processes in these cases (although it should be noted that the 20° detector was not used for the highest fusion power discharges shown in Fig. 9, to avoid possible probe damage due to disruptions).

The time dependence of the alpha loss rate per neutron at these other three detectors was also generally similar to that of the 90° data (as in Figs 7 and 8). However, in some discharges, there was a gradual increase over the whole duration of the NBI pulse in the loss rate at the 20° detector, and to a lesser extent at the 45° detector. The mechanism for these slow increases in the normalized alpha losses at 20° and 45° is not yet understood, but might be due to a diffusive component of TF ripple loss [22]. Note that this is not the same as the ‘delayed loss’ seen previously [12], since that loss was seen only in the 90° detector, and was not seen in DT (see Section 6.2).

The normalized alpha loss versus plasma current in the 60° detector behaved like that at 90° , in that it generally decreased with plasma current from $I = 0.6$ MA to 2.5 MA, similar to the predictions of the first orbit model. However, alpha loss at the 45° detector gradually decreased by $\approx 30\%$ between $I = 1.8$ MA and $I = 0.6$ MA, instead of increasing by a factor of 3 as predicted by the Lorentz orbit code [23]. Since the DD data for this detector show the same trend versus plasma current as the DT data, this was clearly not a new ‘collective’ alpha effect, but rather a non-first-orbit ‘single particle’ loss process common to DD and DT fusion products. A somewhat similar behaviour was seen for the DT alpha collection fraction in the 20° detector, which decreased from $I = 1.0$ MA to $I = 0.6$ MA, similar to previous DD results obtained with the 20° probe [15, 22].

A more complete analysis of these signals will be presented elsewhere, along with modelling of the collisional TF ripple loss effects, which may help explain the non-first-orbit loss effects seen in the 45° and 20° detectors (see Appendix B).

6. SUMMARY AND DISCUSSION

This paper described measurements and analysis of DT alpha particle loss in TFTR, concentrating on the detector located at the vessel bottom in the ion ∇B drift direction. In general, the DT alpha particle loss processes were similar to those previously seen for DD fusion products. No new ‘collective’ alpha particle loss processes have yet been observed. A discussion in terms of the various alpha loss mechanisms is given below.

6.1. First orbit loss

The alpha loss data for the 90° detector was entirely consistent with the simple first orbit loss model. For example, the alpha collection fraction at fixed plasma current was independent of the DT neutron rate, as expected for a ‘single particle’ loss mechanism, and the pitch angle and gyroradius distributions agreed well with the calculated first orbit loss. The plasma current dependence of the alpha loss was also consistent with the first orbit loss model for this 90° detector. However, the alpha loss in the 45° and 20° detectors was not consistent with the first orbit loss model alone, perhaps owing to the additional effects of TF ripple induced alpha loss.

6.2. Delayed loss

The ‘delayed loss’ routinely seen in the 90° detector at high plasma current in DD discharges was much reduced or absent for DT alphas. This was illustrated in Section 4.9 for plasmas with $I = 2.0$ MA, which had a relatively small delayed loss in DD. A clearer example of the absence of delayed loss in DT is shown in Fig. 19 for $I = 2.5$ MA plasmas, for which the delayed loss in DD was relatively larger [12]. This absence of delayed loss in DT also occurred for the (few) $R = 2.45$ m plasmas made so far, which tended to have a larger delayed loss in DD than discharges at $R = 2.52$ m [16].

The absence of delayed loss in DT suggests that it might be caused by a collisional ‘single particle’ effect, since the collisionality changes significantly between DD tritons and DT alphas, whereas the gyroradius dependent first orbit loss and the collisionless TF ripple loss do not. For example, the ratio of the pitch angle scattering time to the energy e folding time for 1 MeV tritons is only ≈ 2 , whereas for alpha particles it is ≈ 15 [16], i.e. tritons accumulate more pitch angle scattering over their slowing down time than alphas,

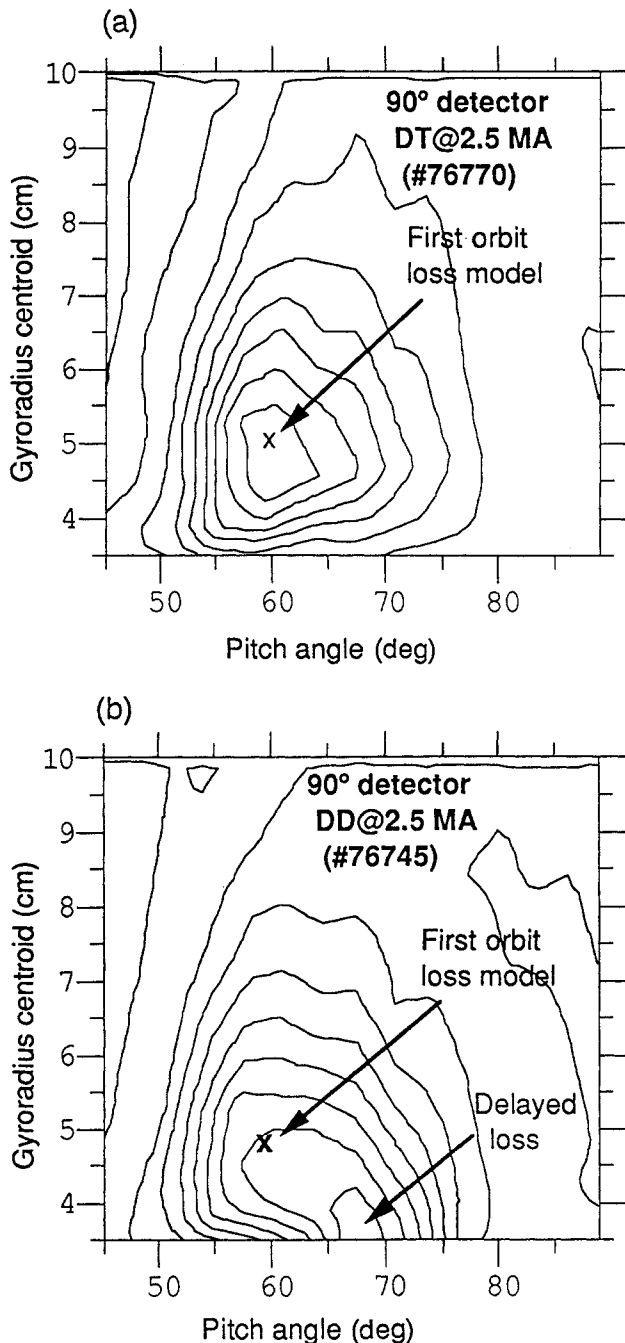


FIG. 19. Comparison between the pitch angle versus gyroradius distributions of (a) DT discharges and (b) DD discharges at $I = 2.5$ MA. The delayed loss component in DD at $\chi \approx 65$ – 70° pitch angle and $\rho \approx 3$ – 4 cm gyroradius is not seen in DT. The most likely cause is the difference in classical pitch angle scattering between 1 MeV tritons in DD and 3.5 MeV alphas in DT.

and so presumably have more collisional loss (this ratio is ≈ 25 for 3 MeV protons).

The theory of classical collisional pitch angle scattering into the first orbit loss cone has recently been

developed and applied to TFTR [24]. However, quantitative predictions have not yet been made for the collisional loss fraction to the local 90° detector for the DT versus DD fusion products.

6.3. TF ripple loss

Previous study of DD fusion product loss to the 20° detector showed a fairly good agreement between the measurements and the collisionless stochastic TF ripple diffusion model incorporated into the MAPLOS code [15, 22]. A comparable study of the 20° detector signals for DT alphas has not yet been made. The modelling of TF ripple loss also needs to be improved to incorporate collisional effects [25]. Since alpha ripple loss is an important consideration for the design of the first wall of ITER [1], specific DT experiments on alpha ripple loss are also planned.

6.4. MHD induced loss

There was no significant time averaged increase in the alpha loss associated with background plasma MHD activity in the DT discharges analysed for this paper (i.e. those in Table I). On the basis of scatter and uncertainties in the data shown in Figs 9 and 10, an *upper limit* to potential MHD induced loss at $I \geq 1.8$ MA in this data set is roughly $\approx 50\%$ of the first orbit loss level. This is less than the MHD induced fusion product loss previously observed in DD, where large coherent MHD activity often increased the fusion product loss by up to a factor of 3 at $I \geq 1.6$ MA [13, 16].

This apparently lower level of MHD induced alpha loss in DT was partially due to the intentionally lower level of MHD activity in many of these DT discharges, such as those in the moderate power plasma current scan at $I = 0.6$ – 1.8 MA and those in the modest power alpha heating experiment at $I = 1.8$ MA, which were designed to avoid MHD activity. However, in general, the level of background plasma MHD activity in DT plasmas was similar to that in DD plasmas with similar plasma parameters [26], and there have been many examples in DT (beyond the scope of the present database) that have shown transient MHD induced alpha loss during sawteeth, fishbones, coherent modes and minor disruptions, all of which appear to be at least qualitatively similar to behaviour previously seen in DD. These results will be described and analysed in detail elsewhere.

It should be noted that it is more difficult to identify relatively low levels of MHD induced fluctuations in the fusion product loss since the change to the dimmer

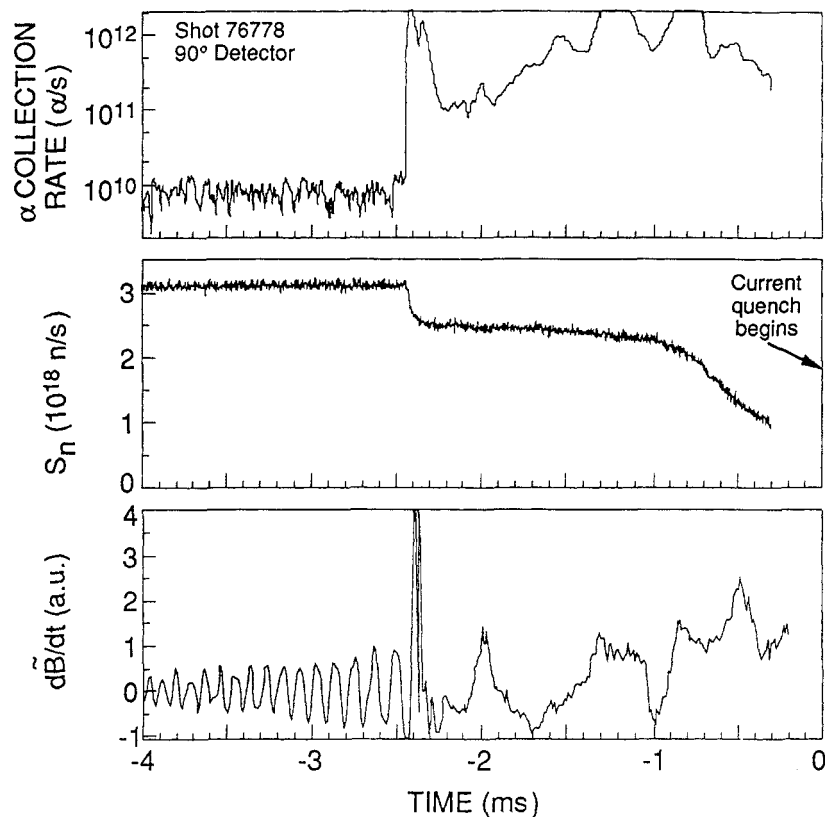


FIG. 20. A discharge in which there was a large increase in DT alpha particle loss just prior to a major disruption, with $I = 2.5$ MA, 33 MW of NBI and 9.2 MW of fusion power (No. 76778). The plasma current has not changed during this time, but large MHD activity was observed. Smaller increases in alpha loss were seen in the other detectors. Similar disruption induced fusion product loss was seen in DD discharges.

P46 scintillators after the 1992 run. This is because the signal per fusion product decreased by about a factor of 20, whereas the neutron/gamma background in the fiberoptic bundle per neutron remained the same, causing a relatively larger background level and so a larger level of background fluctuations that can mask small MHD induced alpha loss (see Section 2). Thus, there may be relatively low levels of MHD induced loss in the DT data described here that were not measurable, for example, at the level of ≈ 10 – 20% of the first orbit loss level.

By far the clearest MHD induced loss observed during DT has been during major disruptions, as illustrated in Fig. 20. In this discharge the alpha loss increased by more than a factor of 100 during the ‘thermal quench’ period ≈ 2 ms just before the plasma current started to decay. The complicated time dependence of the alpha loss during this disruption is probably due to the kink and ballooning mode MHD observed during this time [26]. Similar behaviour was

seen previously during disruptions in DD [16], so there is no reason to believe that this DT loss is a collective alpha effect.

It is interesting that the relative increase in the alpha loss at the 90° detector in this disruption was much larger than that in the 60° or 45° detectors, as if the alpha loss during disruption was mainly in the vertical (∇B) direction. It was estimated that in this discharge a total of $\approx 10\%$ of the confined alphas were lost prior to the current quench. Such an alpha loss mechanism may be a concern for the design of the ITER first wall.

6.5. Collective alpha effects

No alpha particle losses due to any new ‘collective’ alpha instabilities were observed in the DT experiments analysed in this paper [5]. This is not too surprising, since no other symptoms of any such alpha driven instabilities were observed in these cases. For

example, the level of the Alfvén activity measured in these DT discharges was much smaller than that seen during the TAE mode experiments with NBI or ICRH minority ions in TFTR DD plasmas [26]. Those experiments that did generate TAE modes in DD plasmas did have an associated loss of NBI or minority tail ion loss, which is discussed elsewhere [27], but since those instabilities were not driven by alpha particles, the self-consistent non-linear-alpha-particle-wave interaction could not be studied directly. Future collective alpha experiments in DT are reviewed in Section 6.6.

6.6. Conclusions

Alpha particle loss was measured during the first year of the TFTR DT run with a detector 90° below the outer midplane in the ion ∇B drift direction. The alpha loss seen in this detector during DT was dominated by the classical ‘single particle’ first orbit loss process. No signs of any new ‘collective’ alpha particle loss processes were seen up to the maximum fusion power level of 10.7 MW, i.e. the alpha collection fraction at a constant plasma current was independent of the DT neutron rate up to an alpha source power level of ≈ 2 MW. This was also true for the alpha signals seen in the other alpha loss detectors (described only briefly here).

In addition to the absence of any collective alpha loss process, these initial DT results also show a relatively lower level of MHD induced loss and ‘delayed loss’ than the corresponding DD discharges [13, 16]. One possible explanation for this could be based on the different single particle collisionality of 3.5 MeV alphas and the 1 MeV triton fusion product. The DD tritons have a ≥ 3 times longer slowing down time than DT alphas, so that the confined triton population susceptible to MHD or delayed loss is larger than that for alphas, relative to their comparable first orbit loss fractions. The tritons also have a larger pitch angle scattering over their thermalization time, potentially leading to increased collisional loss [24].

Further data analysis is needed in several areas before drawing any final conclusions concerning alpha particle loss in TFTR DT. In particular, more work is needed to analyse the alpha loss to the detectors at 60 , 45 and 20° below the outer midplane, and to correlate this loss with calculations of the expected collisional TF ripple loss. The MHD induced alpha loss effects that have been seen in some cases also need to be examined and modelled more carefully.

Further work is also needed to try to excite collective alpha particle driven instabilities in TFTR, and

several experiments in this area are in progress. The alpha particle population can be increased by lengthening the time over which the fusion power is maximized, perhaps by raising further the toroidal field to reduce MHD instability. ICRH is being added to heat the electrons to increase the alpha slowing down time and therefore to increase the steady state alpha population. Attempts are being made to destabilize TAE modes by decreasing the ion Landau damping (by transiently reducing the ion temperature), by increasing the alpha particle drive by raising $q(0)$ (to move the TAE gaps nearer the alpha pressure gradient), and by increasing the plasma beta (to drive ‘BAE’ modes). So far none of these techniques has created a clear alpha driven mode in which the alpha particle transport loss can be studied, so this is still a goal for the TFTR DT programme.

Appendix A

CALCULATIONS OF GLOBAL ALPHA LOSS

The global (i.e. total) alpha loss fractions for some of the TFTR discharges of Table I were calculated using several different codes, with the results shown in Fig. 21. These global loss calculations were not directly used for interpreting the local alpha loss measurements described in this paper, but are described here for the sake of completeness. The actual local measurements were compared with a Lorentz code (Section 3), which takes into account the solid angle of the detector acceptance and the decrease in the angle of the orbit’s trajectory towards the wall with increased plasma current. These effects are not taken into account in the calculations described in this Appendix, for example, only the total alpha loss per unit wall area was calculated.

The MAPLOS code [15] was used to calculate the first orbit and TF ripple loss using 256 000 ions in a collisionless bounce averaged orbit-following Monte Carlo code in a simplified magnetic geometry. The SNAP code calculated the guiding centre orbits of ≈ 2000 alpha particles born on a poloidal, radial and pitch angle grid using its own model for the plasma current and alpha source profile. Both these models counted alphas hitting the wall in a single orbit as first orbit loss, and confined trapped alphas whose first banana tips lay in the stochastic TF ripple loss region were counted as TF ripple loss, as in the RIPLOS code [28]. The TRANSP code [29] follows a Monte Carlo distribution of ≈ 6000 alpha orbits calculated using its

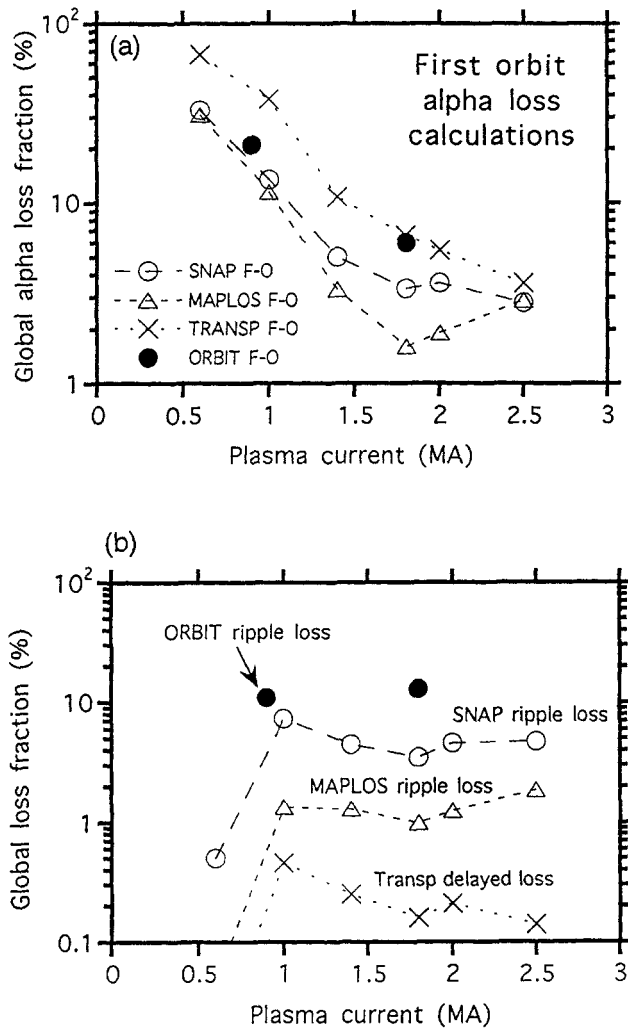


FIG. 21. Calculations of the global (i.e. total) alpha particle loss in TFTR versus plasma current from various codes for some of the discharges of Table I. The first orbit loss calculations (a) agree reasonably well with each other, the main differences being due to slightly different modelling of the discharge profiles and wall. The calculated TF ripple loss (b) increases substantially between collisionless and collisional models, but the collisional axisymmetric losses are small, according to TRANSP.

version of the alpha source and plasma current profiles, including a model for collisional slowing down and pitch angle scattering, but not TF ripple.

These codes are in agreement that the first orbit alpha loss at $I = 0.6$ MA is $\approx 40 \pm 20\%$, while at $I = 2.0$ MA it is $\approx 4 \pm 2\%$. The differences between codes for a given plasma current are partly due to their somewhat different assumptions for the alpha source

and plasma current profiles. The TRANSP first orbit loss results [29] are somewhat higher than those of the other codes, probably because it assumes that the vessel wall is closer to the plasma edge (this is modelled more correctly in the other codes).

The TF ripple loss calculated from the collisionless MAPLOS and SNAP codes is $< 1\%$ at $I = 0.6$ MA, since few trapped alphas were confined on their first orbits, and $\approx 5\%$ from both codes at $I = 2.0$ MA. However, the collisional TF ripple induced alpha loss as calculated by the Monte Carlo guiding centre code ORBIT was $\approx 20\%$ [25], i.e. much larger than the collisionless alpha loss. Note that these ORBIT calculations were done only for higher ripple plasmas with $R = 2.6$ m, and were limited to ≈ 250 alpha particles.

MAPLOS calculations of the poloidal distribution integrated over pitch angle of alpha loss for the $I = 0.6$ MA and $I = 2.0$ MA cases are shown in Fig. 22. The first orbit loss was predicted to be broadly distributed in the poloidal direction, whereas the TF ripple loss is predicted to be highly localized near the outboard midplane [15, 22]. The poloidal distribution integrated over pitch angle of TF ripple induced alpha loss determined by the collisional ORBIT for one case ($I = 1.8$ MA, $R = 2.6$ m) was similar to that obtained by MAPLOS, i.e. the TF ripple induced alpha loss is localized to within $\leq 30^\circ$ of the outboard midplane [25]. Therefore TF ripple induced alpha loss should not be visible in the 90° lost alpha data analysed in this paper.

Several other fusion product loss mechanisms have been investigated recently. Calculations of axisymmetric collisional loss, due to pitch angle scattering of alphas born near the passing/trapped boundary into the first orbit loss cone, have been made using a simplified analytic model and compared with the Monte Carlo calculations in TRANSP [24]. The calculated poloidal distribution of collisional loss (without TF ripple) was similar to that of first orbit loss, i.e. peaked near the bottom of the vessel, but the magnitude of this loss was much less than that of first orbit loss (Fig. 21). This is consistent with earlier calculations of non-prompt alpha loss [30].

The effect of helical magnetic perturbations due to internal plasma MHD activity on alpha loss has been calculated previously using the GC3 code [16, 31]. However, in the DT experiments described in this paper there was no observable MHD induced increase in the alpha loss, except during disruptions (Section 6.4). ICRH induced loss has been observed and modelled in DD plasmas [32], but the present experiments did not have any ICRH.

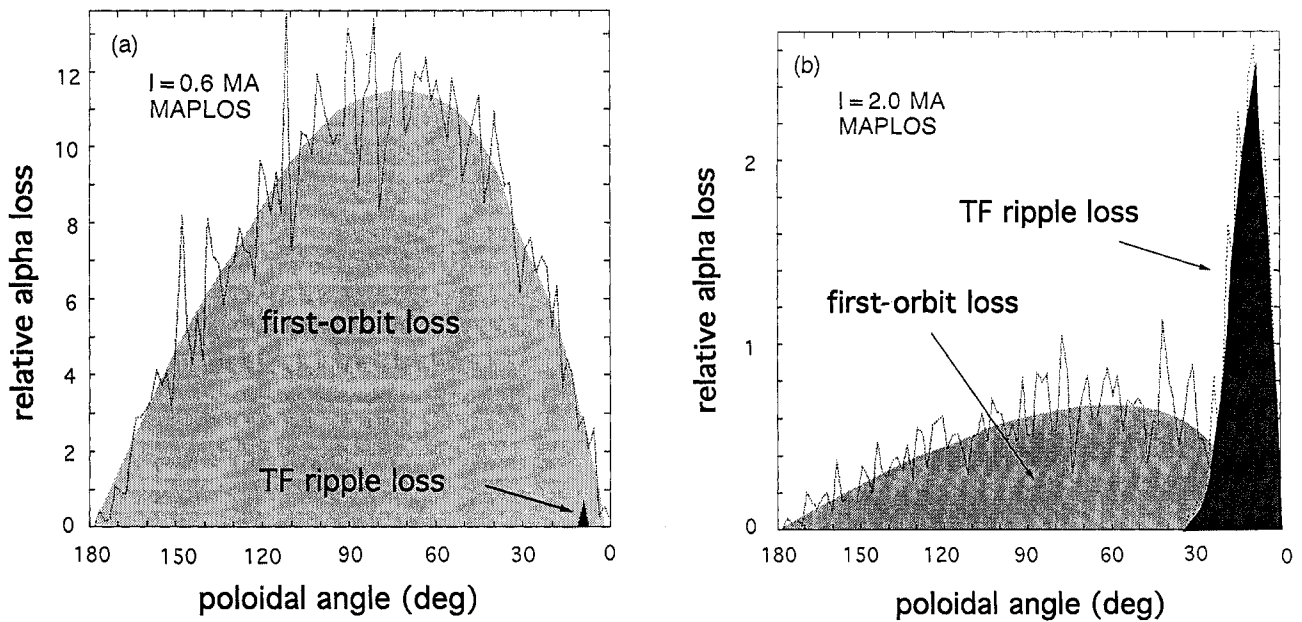


FIG. 22. Calculations of the shapes of the poloidal distributions of 3.5 MeV alpha loss at the wall in TFTR based on the MAPLOS code. The shaded regions represent smoothed approximations to the Monte Carlo results (dotted lines). For both (a) $I = 0.6$ MA and (b) $I = 2.0$ MA the first orbit loss has a broad peak along the vessel bottom between 60° and 90° below the outboard midplane. At $I = 2.0$ MA there is a significant TF ripple induced alpha loss component at $\leq 30^\circ$ below the outboard midplane. The TF ripple loss calculated using the collisional ORBIT code model also predicts alpha loss to be localized $\leq 30^\circ$ below the outboard midplane.

Appendix B

COMPARISON OF TRANSP PROFILES WITH MEASUREMENTS

The calculations of first orbit alpha loss in Section 3 used as input the neutron source profiles $S(r)$ and the $q(r)$ profiles calculated by the time dependent TRANSP transport code [29], which were available for almost all of the discharges discussed in this paper. This Appendix gives some typical comparisons between the TRANSP calculations and the measurements of these quantities that were available for some of the discharges discussed in this paper.

A comparison between the measured $S(r)$ profile and the TRANSP modelling of this profile is shown in Fig. 23 for one of the $I = 1.8$ MA high powered DT discharges (No. 73346). For this comparison the TRANSP profile was integrated over nine vertical chords for a direct comparison with the lines of sight of the vertical multichannel neutron collimator [33]. The agreement is fairly good for both the profile shape and the absolute neutron emission level.

The Abel-inverted neutron source profiles from the neutron collimator data were calculated and read into the Lorentz orbit code, and the alpha collection fraction was calculated in the same way as for

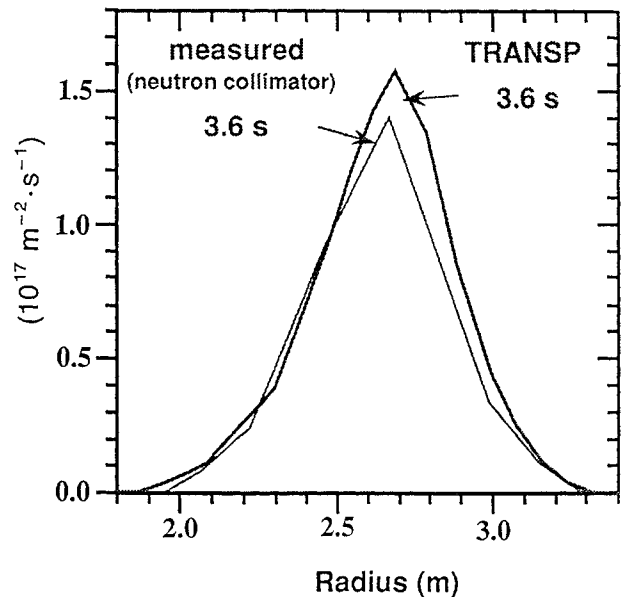


FIG. 23. Comparison of the TRANSP calculations of the DT neutron source profile with measurements from the vertical neutron collimator for a high power DT discharge at $I = 1.8$ MA (No. 73446). In both cases the neutron emission is integrated over a vertical chord corresponding to the detector location. The small differences between the two profiles result in a $\approx 15\%$ change in the calculated first orbit loss to the 90° detector for this discharge.

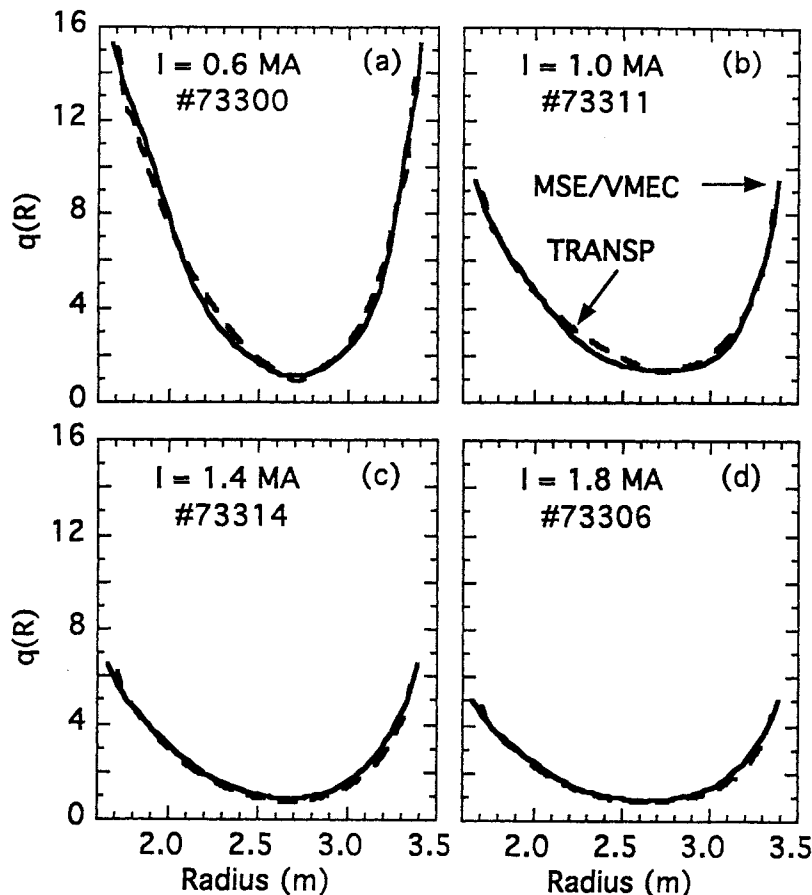


FIG. 24. The $q(R)$ profiles at 0.6 s after the start of NBI computed by VMEC from the MSE measurements (solid lines), and by TRANSP (dashed lines) for single tritium source shots at $I = 0.6$ – 1.8 MA.

the TRANSP neutron profiles, while keeping the magnetic configuration constant. The resulting first orbit alpha collection fraction for the 90° detector was $\approx 15\%$ higher than for the TRANSP neutron source profile for this case, which is within the estimated $\approx 30\%$ uncertainty in the calculation of this loss. Similar variations in the neutron source profiles at lower plasma current would result in a smaller change in resulting alpha collection fraction, as discussed in Section 3.

The calculations of alpha collection fractions also depended on the TRANSP calculated $q(r)$ profiles. A consistency check of TRANSP was made using data from the MSE diagnostic [34]. The MSE diagnostic measures the internal magnetic field pitch angle profile at up to 12 locations in the midplane of the tokamak. These data, along with external magnetic field and internal kinetic profile information (including fast particle effects), were used by the free boundary equilibrium code VMEC [35] to find a self-consistent magnetohydrodynamic equilibrium.

The $q(R)$ profiles computed by VMEC and by TRANSP are shown in Fig. 24 for the discharges at four different plasma currents (from Table I). For plasma currents greater than $I = 0.6$ MA, the two calculations differed by less than 20%. From Monte Carlo analysis of the entire MSE/VMEC data analysis procedure, it was estimated that the uncertainty in $q(0)$ was 7%, while the uncertainty in the rest of the profile was less than 10% [36]. A similar error analysis of the TRANSP q profile has not yet been performed.

The Lorentz orbit code was used to calculate the first orbit alpha collection fraction using both the MSE/VMEC and TRANSP $q(r)$ profiles, which were derived by symmetrizing the $q(R)$ profiles, while keeping the neutron source profile fixed. As shown in Fig. 25, the results for all currents were within $\approx 10\%$ of each other, which was well within the estimated $\approx 30\%$ uncertainty in this calculation. Thus the TRANSP calculated q profiles were sufficiently accurate for calculations of the alpha collection fraction. Such good

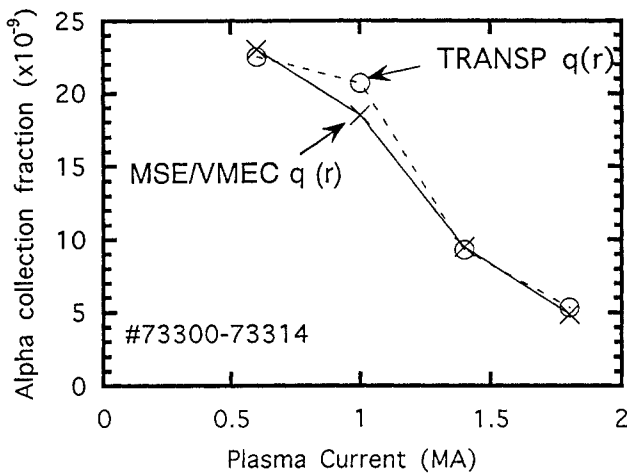


FIG. 25. First orbit alpha collection fraction versus current computed using either the symmetrized MSE/VMEC $q(r)$ profile (solid line) or the TRANSP $q(r)$ profile (dashed line). The difference between the two is less than 10%.

agreement between VMEC and TRANSP was not typical. The agreement in these discharges occurs because these cases do not have significant MHD activity, sawteeth or non-inductive current, all of which can cause substantial deviations from the TRANSP results.

ACKNOWLEDGEMENTS

We thank C.W. Barnes, M. Bell, C.E. Bush, R.L. Boivin, C.Z. Cheng, M. Diesso, H. Duong, J. Felt, G.Y. Fu, H.P. Furth, G. LeMunyan, R.J. Hawryluk, W.W. Heidbrink, D.W. Johnson, K. McGuire, D.M. Meade, D.A. Spong, M. Tuszewski, V. Yavorski and R.B. White for their various contributions and support for this work, which was performed under USDOE Contract No. DE-AC02-76CHO-3073.

REFERENCES

- [1] PUTVINSKI, S., et al., in Plasma Physics and Controlled Nuclear Fusion Research 1994 (Proc. 15th Int. Conf. Seville, 1994), Vol. 2, IAEA, Vienna (1995) Paper E-P4.
- [2] HEIDBRINK, W.W., SADLER, G.J., Nucl. Fusion **34** (1994) 535.
- [3] CHENG, C.Z., et al., in Plasma Physics and Controlled Nuclear Fusion Research 1992 (Proc. 14th Int. Conf. Würzburg, 1992), Vol. 2, IAEA, Vienna (1993) 51.
- [4] ZWEBEN, S.J., Nucl. Fusion **28** (1988) 2230.
- [5] STRACHAN, J.D., et al., Phys. Rev. Lett. **72** (1994) 3526.
- [6] HAWRYLUK, R.J., et al., Phys. Rev. Lett. **72** (1994) 3530.
- [7] BOVIN, R., et al., Rev. Sci. Instrum. **63** (1992) 4418.
- [8] ZWEBEN, S.J., Rev. Sci. Instrum. **63** (1992) 4565.
- [9] TUSZEWSKI, M., ZWEBEN, S.J., Rev. Sci. Instrum. **64** (1993) 2459.
- [10] DARROW, D.S., et al., Rev. Sci. Instrum. **66** (1995) 476.
- [11] ZWEBEN, S.J., et al., Nucl. Fusion **31** (1991) 2219.
- [12] ZWEBEN, S.J., et al., Nucl. Fusion **33** (1993) 705.
- [13] ZWEBEN, S.J., et al., in Plasma Physics and Controlled Nuclear Fusion Research 1992 (Proc. 14th Int. Conf. Würzburg, 1992), Vol. 1, IAEA, Vienna (1993) 363.
- [14] ZWEBEN, S.J., et al., Nucl. Fusion **30** (1990) 1551.
- [15] BOIVIN, R.L., et al., Nucl. Fusion **33** (1993) 449.
- [16] ZWEBEN, S., et al., Phys. Plasmas **1** (1994) 1469.
- [17] FELT, J., et al., Rev. Sci. Instrum. **61** (1990) 3262.
- [18] RAMSEY, A.T., Rev. Sci. Instrum. **66** (1994) 871.
- [19] JOHNSON, L.C., et al., Rev. Sci. Instrum. **66** (1995) 894.
- [20] DUONG, H.H., et al., Nucl. Fusion **33** (1993) 749.
- [21] SIGMAR, D.J., et al., Phys. Fluids B **4** (1992) 1506.
- [22] BOIVIN, R.L., ZWEBEN, S.J., Phys. Fluids B **5** (1993) 1559.
- [23] ZWEBEN, S.J., in Controlled Fusion and Plasma Physics (Proc. 21st Eur. Conf. Montpellier, 1994), Vol. 18B, Part I, European Physical Society, Geneva (1994) 290.
- [24] CHANG, C.S., et al., Phys. Plasma **1** (1994) 3857.
- [25] REDI, M.H., et al., Collisional Stochastic Ripple Diffusion of Alpha Particles and Beam Ions on TFTR, Rep. PPPL-3011, Princeton Plasma Phys. Lab., NJ (1994).
- [26] FREDRICKSON, E.D., et al., in Plasma Physics and Controlled Nuclear Fusion Research 1994 (Proc. 15th Int. Conf. Seville, 1994), Vol. 1, IAEA, Vienna (1995) Paper A2-10.
- [27] DARROW, D.S., et al., in 1992 International Conference on Plasma Physics (Proc. Conf. Innsbruck, 1992), Vol. 16C, Part I, European Physical Society, Geneva (1992) 431.
- [28] WHITE, R.B., MYNICK, H.E., Phys. Fluids B **1** (1989) 980.
- [29] BUDNY, R.V., Nucl. Fusion **34** (1994) 1247.
- [30] HIVELY, L.M., MILEY, G.H., Nucl. Fusion **20** (1980) 969.
- [31] MYNICK, H.E., Phys. Fluids B **5** (1993) 1471.
- [32] DARROW, D.S., et al., ICRF-Induced Fusion Product Losses in TFTR, Rep. PPPL-2975, Princeton Plasma Phys. Lab., NJ (1994).
- [33] ROQUEMORE, A.L., et al., Rev. Sci. Instrum. **66** (1995) 916.
- [34] LEVINTON, F.M., Rev. Sci. Instrum. **63** (1992) 5157.
- [35] HIRSHMAN, S.P., et al., Phys. Plasmas **1** (1994) 2277.
- [36] BATHA, S.H., et al., Rev. Sci. Instrum. **66** (1995) 372.

(Manuscript received 9 December 1994
Final manuscript accepted 14 February 1995)